THE ASTROPHYSICAL JOURNAL, 386:375–397, 1992 February 20

A SELF-CONSISTENT FIELD METHOD FOR GALACTIC DYNAMICS

LARS HERNQUIST[1]
Lick Observatory, U.C. Santa Cruz, CA 95064

AND

JEREMIAH P. OSTRIKER
Princeton University Observatory, Princeton, NJ 08540
Received 1991 May 31; accepted 1991 August 26

ABSTRACT

An algorithm for evolving collisionless stellar systems is described. Our approach is similar to that suggested earlier by van Albada, McGlynn, and more specifically Clutton-Brock, in that Poisson's equation is solved by expanding the density and potential in a set of basis functions. However, the basis set used here is constructed so that the lowest order members well-approximate a galaxy obeying the de Vaucouleurs $R^{1/4}$ law in projection. Consequently, it will be possible to study the evolution of systems with density profiles like the $R^{1/4}$ law using only a few terms in the expansions. A good fit is also obtained for a truncated isothermal distribution and, so, our method will be quite appropriate for galaxies with flat rotation curves.

Since our method is similar in spirit to solving N one-body problems, the cpu cost scales with particle number as $O(N)$ with a relatively small coefficient. Hence, calculations employing $N \sim 10^6$–10^7 are straightforward on existing supercomputers, making possible simulations having significantly smoother fields than with direct methods such as tree-codes. Even larger N should be feasible on multiple-cpu computers since opportunities for parallelism abound.

Moreover, the flexibility of the algorithm suggests a number of refinements that may suppress discreteness noise relative to direct N-body methods. Owing to its one-body character, our method lends itself to an iterative technique akin to those utilized by Ostriker and collaborators for nonspherical stars and by Schwarzschild for equilibrium stellar-dynamical systems. In the present context, one finds orbits in a given static or time-dependent gravitational field and then, from the resultant density, $\rho(\mathbf{r}, t)$, revises the potential, $\varphi(\mathbf{r}, t)$. However, because of Poisson noise in the representation of the density field, the convergence properties of this scheme are problematic.

Possible scientific uses of our technique are discussed, including tidal perturbations of dwarf galaxies, the adiabatic growth of central masses in spheroidal galaxies, instabilities in realistic galaxy models, and secular processes in galactic evolution.

Subject headings: celestial mechanics, stellar dynamics — methods: numerical

1. INTRODUCTION

Stellar systems such as galaxies are "collisionless" to a high degree of precision over their typical dynamical time scales. In fact, normal galaxies are collisionless for times much longer than a Hubble time. This means that individual stars follow orbits in the mean gravitational field generated by the other stars, but are not perturbed by direct interaction with one another. The situation in the solar neighborhood, where the dynamical time is $\sim 10^{8.5}$ yr and the two-body relaxation time is $\sim 10^{14}$ yr, is typical. Some aspects of the dynamics of star clusters can also be studied in the collisionless limit, although relaxation effects become significant at late stages of the evolution of globular clusters.

Gravitating systems which are effectively collisionless satisfy the coupled Vlasov and Poisson equations. If $f_i(\mathbf{r}, \mathbf{v})$ is the distribution function for any species i having particle mass m_i, then

$$\frac{\partial f_i}{\partial t} + \mathbf{v} \cdot \nabla f_i - \nabla\varphi \cdot \nabla_v f_i = 0 \,, \tag{1.1}$$

$$\nabla^2\varphi = 4\pi G\rho(\mathbf{r}) \equiv 4\pi G\bar{m}(\mathbf{r})n(\mathbf{r}) \,, \tag{1.2}$$

where the mean particle mass $\bar{m}(\mathbf{r})$ is

$$\bar{m}(\mathbf{r}) \equiv \frac{1}{n(\mathbf{r})} \sum_i m_i \int f_i(\mathbf{r}, \mathbf{v}) d\mathbf{v} \,, \tag{1.3}$$

[1] Alfred P. Sloan Foundation Fellow.

the number density of particles $n(\mathbf{r})$ is

$$n(\mathbf{r}) \equiv \sum_i n_i(\mathbf{r}) , \tag{1.4}$$

$$n_i(\mathbf{r}) = \int f_i(\mathbf{r}, \mathbf{v}) d\mathbf{v} , \tag{1.5}$$

$\mathbf{a} = -\nabla\varphi$ is the acceleration, and ∇_v denotes a gradient with respect to velocities. The solution of equations (1.1) and (1.2) as both an initial value and a boundary value problem on a mesh is not feasible in six-dimensional phase space owing to memory limitations of presently available computers. Instead, phase space is sampled using a Monte-Carlo approach in which selected "fluid" elements are integrated forward in time along the characteristic curves of equation (1), defined by

$$\frac{d\mathbf{x}}{dt} = \mathbf{v} , \tag{1.6}$$

$$\frac{d\mathbf{v}}{dt} = \mathbf{a} . \tag{1.7}$$

Computationally, these fluid elements of phase density are represented as particles whose coordinates are advanced using the potential computed from their mass density. Note that equation (1.1) is valid for *any* set of test particles orbiting in the potential φ.

A common, albeit naive, approach is to represent the density by a small set of equal-mass super-particles: a large-scale simulation might represent 10^{11} stars with 10^5 particles each having a mass $10^6\ M_\odot$. Then one iteratively solves equations (1.6) and (1.7) for each super-particle and Poisson's equation in either the form (1.2) or its integral equivalent.

There are two difficulties with this classic approach. First, since there are $N(N-1)/2$ pairs of orbiting particles, it can be computationally expensive. The cost can be reduced to $\sim O(N \log N)$ by schemes such as tree-codes (Barnes & Hut 1986; Hernquist 1987), which are efficient at solving Poisson's equation, but, even so, interactions between nearby particles will be expensive to compute when high resolution is required. The second, closely related problem is that of relaxation. Since the potential is inherently "grainy" in the N-body approach, two-body encounters will alter the distribution function in ways that violate equation (1.1).

Often such alteration is harmless and many important results for collisionless stellar systems have been obtained with N-body codes. Among these are studies of the stability of galaxy models where the relevant evolution proceeds much more rapidly than relaxation effects (e.g., Ostriker & Peebles 1973; Merritt & Aguilar 1985; Barnes, Goodman, & Hut 1986; Merritt & Hernquist 1991; Weinberg 1991). But, there are situations where even small amounts of relaxation can be harmful. Consider two examples. If a thin galactic disk is to be modeled, the velocity dispersion ($\sigma \sim 25$ km s^{-1}) may be very small compared to the rotation velocity ($v_{\rm rot} \sim 250$ km s^{-1}). In such a "cold" system, with a dimensionless "temperature" $t \equiv \sigma^2/\varphi \approx 10^{-2}$, even a small leak, due to relaxation, transferring rotational energy into random energy by two-body scattering can produce serious errors in the velocity dispersion. Another situation obtains in elliptical systems where the presence of nonstandard integrals is required to maintain a triaxial shape. Two-body interactions will scatter orbits from one family to another and tend to produce, locally, an isotropic velocity dispersion which, in turn, prevents maintenance of triaxiality.

For these reasons, it is desirable to formulate efficient techniques that allow one, as closely as possible, to approach the true "collisionless" limit. Since orbital fluctuations are induced by perturbations in the gravitational force (integration schemes are sufficiently refined so as to produce negligible "integration scattering"), the heart of the problem is to find an appropriate means of solving Poisson's equation.

A variety of algorithms have been proposed to compute the gravitational potential. In the "N-body" approach, particles interact with one another directly. The simplest of such techniques is the particle-particle (PP) method in which the potential is obtained by simply summing over all individual pair-wise interactions; e.g.,

$$\varphi(\mathbf{r}_i) = -G \sum_j m_j \frac{1}{(|\mathbf{r}_i - \mathbf{r}_j|^2 + \epsilon^2)^{1/2}} , \tag{1.8}$$

where the softening length, ϵ, prevents numerical divergences when two particles pass close to one another. (For present purposes, tree-codes [e.g., Barnes & Hut 1986; Hernquist 1987] are essentially identical to PP schemes.) The softening of the potential, parameterized by ϵ, is necessary to prevent excessive computer investment in close encounters but it limits one's ability to accurately represent small regions such as a galactic center or disk.

A feature common to N-body methods is that particles interact with one another as if they are physical objects; i.e., softened point-masses. Consequently, the potential obtained by an N-body method is fundamentally that appropriate to a collection of N gravitating bodies and is not necessarily a good representation of the mean gravitational field of a collisionless system.

The fact that particles interact with one another individually in N-body codes implies that two-body effects are not obviously negligible for finite N. In three dimensions, equal logarithmic intervals in impact parameter contribute equally to gravitational scattering and thus softening suppresses relaxation effects to only a modest degree.

Another approach is to solve Poisson's equation by expanding the density and potential in a set of basis functions. If the first few members of the basis set provide a good approximation to the global structure of the system being studied, the expansion can be truncated at relatively low order with negligible error. In so doing, one intentionally discards all knowledge of the small-scale structure of the system, and parameterizes the field in such a way that additional refinements may make it possible to mitigate

relaxation effects arising from local discreteness noise. The truncation of the expansions has an effect which is analogous to the introduction of softening in direct methods.

This technique has, of course, been suggested and used by a number of earlier workers. Loosely speaking, the various algorithms developed in this context are referred to as "expansion" codes. Some confusion has arisen in the literature concerning their relaxation properties. In most implementations (e.g., Hénon 1964; Aarseth 1967; van Albada & van Gorkom 1977; Fry & Peebles 1980; Villumsen 1982; White 1983; McGlynn 1984) the angular dependence is expanded in spherical harmonics but the radial part of Poisson's equation is solved directly. As is discussed at length in § 5, the result of this procedure is that the particles interact with one another as if they had the shapes of portions of spherical shells (e.g., McGlynn 1984). Softening is introduced either explicitly (e.g., White 1983) or implicitly through a grid (e.g., van Albada & van Gorkom 1977) to prevent numerical divergence when these shells pass by one another.

Codes which rely on angular expansions but solve the radial dependence directly are essentially N-body codes and, as far as collisionless dynamics are concerned, retain some of the undesirable properties of the PP method. For example, relaxation rates in these codes are only mildly suppressed relative to direct methods for a similar effective resolution (Hernquist & Barnes 1990). It is not immediately obvious how to refine the spherical harmonic method to mitigate the effects of discreteness noise.

If, instead, one takes the expansion technique to its full and logical conclusion by also expanding the radial dependence in a set of basis functions, then further refinements can be made to reduce some of these remaining difficulties. In his excellent review of numerical modeling, Sellwood (1987) refers to these methods as "pure" expansions. To avoid confusion with hybrid N-body expansion techniques we choose to instead refer to these approaches as self-consistent field (SCF) methods. This terminology is motivated by analogy with similar algorithms used to construct models of rotating stars (Ostriker & Mark 1968; Ostriker & Bodenheimer 1968) and by the fact that these "pure" expansions are essentially *field* methods. That is, the particles in SCF techniques do not interact with one another directly but only through their contribution to the combined gravitational field of the system. In other words the potential in SCF codes does not depend on relative coordinates of particles.

Another important aspect of the SCF approach is that it is well-suited to an iterative solution of equations (1.1) and (1.2). In the hydrodynamical analog, one uses an estimated density to compute the potential. Then one determines the equilibrium in this external potential. The new equilibrium density provides a new potential which, it has been found, converges iteratively to a self-consistent solution (hence the name "SCF"). In the stellar-dynamical case, we can compute orbits in a given potential in the same fashion as did Schwarzschild (1979, 1982), with the exception that the potential may be fully time-dependent. Then, one can use the computed orbits to find the evolving density distribution, recompute the potential and iterate. Among the many advantages of this approach is that, since all orbits are computed in given potentials $\varphi(\mathbf{r}, t)$ one solves, iteratively N one-body problems rather than one N-body problem. Utilizing modern developments in computational hardware and software, N one-body problems have an inherently parallel structure which can be treated efficiently by new computer architectures.

SCF methods have been used only sparingly in the context of stellar dynamics. As emphasized by Sellwood (1987), it is essential that the lowest order members of the radial basis provide a good global approximation to the system being modeled. Otherwise, it would be necessary to carry out the expansions to high order which would compromise their efficiency. One of the first implementations of an SCF algorithm in computational stellar dynamics was by Clutton-Brock (1972, 1973). In his first paper, Clutton-Brock describes the use of Hankel-Laguerre functions to obtain the potential of flat, i.e., two dimensional, galaxies (see also Aoki & Iye 1978). The second paper, which is more relevant to the discussion here, introduces a basis whose zeroth order members are simply the density-potential pair in Plummer's model (Plummer 1911). Such a basis set is quite attractive for modeling some aspects of the dynamics of globular clusters but is less well-suited for spheroidal galaxies. Allen, Palmer, & Papaloizou (1990) employ a well-known set of basis functions for spheroidal systems of finite extent involving spherical Bessel functions (e.g., Fridman & Polyachenko 1984; Weinberg 1989). Their technique is also not appropriate for studying spheroidal galaxies owing to its limited dynamic range.

In this paper a new set of expansion functions is described and analyzed. It is based on the model for spherical galaxies obeying the $R^{1/4}$ law discussed by Hernquist (1990a). To the extent that Hernquist's model gives a good description of the properties of *spherical* galaxies, the technique presented here will provide a useful method for investigating the dynamics of *spheroidal* galaxies. Our formal development is similar to that of Clutton-Brock (1973, hereafter CB). However, we choose to present our method in some detail since, for reasons not immediately obvious to us, Clutton-Brock's approach has been virtually ignored in the literature. Other expansions may be better suited to flat systems (e.g., Toomre 1963; Yabushita 1969; Clutton-Brock 1972; Kalnajs 1976; Aoki & Iye 1978), and still others to those with more general geometries. The present treatment is intended to be illustrative, but we believe it to be quite efficient for typical centrally concentrated astronomical systems.

In § 2, the analysis relevant to our implementation of the SCF method is presented. Technical considerations are discussed in § 3. A comparison with other complementary schemes is made in § 4. Numerical tests are described in § 5. The strengths and weaknesses of the present algorithm are summarized in § 6, where possible scientific applications are also indicated.

2. FORMULATION

2.1. *Underlying Model*

As indicated in § 1 the utility of SCF method depends critically on the selection of a radial basis whose lowest order members resemble the system being studied. To this end, it is useful to begin by "factoring out" a part of the density and potential that well-approximate the system. The approach taken by CB was to divide out a Plummer model from the mass distribution and expand the remaining density and potential in bi-orthogonal series. We adopt a similar philosophy here but use as our starting point a simple model which provides a good approximation to the luminosity distribution of spherical galaxies.

Consider the density-potential pair

$$\rho(r) = \frac{M}{2\pi}\frac{a}{r}\frac{1}{(r+a)^3}, \tag{2.1}$$

$$\varphi(r) = -\frac{GM}{r+a}, \tag{2.2}$$

where M is the total mass and a is a scale length which is related to the half-mass radius of the model, $r_{1/2}$, by $r_{1/2} = (1+\sqrt{2})a$. As demonstrated by Hernquist (1990a) the dynamical and kinematic properties of this model can be evaluated analytically. Moreover, the properties of this model provide a good approximation to those of the $R^{1/4}$ law. For example, the projected surface brightness is

$$I(R) = \frac{M}{2\pi a^2 \Upsilon (1-s^2)^2}\left[(2+s^2)X(s) - 3\right], \tag{2.3}$$

where $s = R/a$, R is the projected radius, Υ is the constant mass-to-light ratio, and

$$X(s) = \frac{1}{\sqrt{1-s^2}}\,\mathrm{sech}^{-1}\,s \qquad \text{for } 0 \le s \le 1, \tag{2.4}$$

$$X(s) = \frac{1}{\sqrt{s^2-1}}\,\sec^{-1}\,s \qquad \text{for } 1 \le s \le \infty. \tag{2.5}$$

The effective radius, R_e, can be computed from the cumulative surface brightness by integrating equation (2.3) in R, with the result $R_e \approx 1.8153a$ (Hernquist 1990a). The projected surface brightness, $I(R)$, normalized to its value at the effective radius, $I(R_e)$, is shown in Figure 1 as a function of $(R/R_e)^{1/4}$, where it is compared with the same quantity for the $R^{1/4}$ law (de Vaucouleurs 1948). As can be seen from the figure, the agreement between the two is reasonably good: the surface brightness profiles agree to within $\approx 35\%$ for radii in the range of $0.06 \lesssim R/R_e \lesssim 14.5$, which enclosed $\approx 94\%$ the total light of each model.

2.2. *A Basis Set*

The fact that the density and potential in equations (2.1) and (2.2) are each simple analytic functions of r suggests that an analysis similar to that employed by CB for the Plummer model be attempted.

Assume the existence of a bi-orthogonal basis set for the density and potential, so that they may be expanded in the series:

$$\rho(\mathbf{r}) = \sum_{nlm} A_{nlm}\rho_{nlm}(\mathbf{r}), \tag{2.6}$$

$$\Phi(\mathbf{r}) = \sum_{nlm} A_{nlm}\Phi_{nlm}(\mathbf{r}), \tag{2.7}$$

where n is the radial "quantum" number and l and m are corresponding quantities for the angular variables. More generally, the two sums will involve different expansion coefficients. The assumption of bi-orthogonality ensures a one-to-one relationship between those terms appearing in the expansions for the density and potential. In addition, the individual harmonics ρ_{nlm} and Φ_{nlm} satisfy Poisson's equation

$$\nabla^2\Phi_{nlm}(\mathbf{r}) = 4\pi\rho_{nlm}(\mathbf{r}). \tag{2.8}$$

Take the zeroth order terms in the expansion to be those of the underlying model we wish to expand about. That is, choose

$$\rho_{000} \equiv \frac{1}{2\pi}\frac{1}{r}\frac{1}{(1+r)^3}, \tag{2.9}$$

and

$$\Phi_{000} \equiv -\frac{1}{1+r}, \tag{2.10}$$

where a dimensionless system of units with $G = 1$, $M = 1$, and $a = 1$ has been adopted.

Following standard practice, expand the angular dependence of ρ_{nlm} and Φ_{nlm} in spherical harmonics, $Y_{lm}(\theta, \phi)$. Next, write the $n = 0$ terms in the expansion of the potential in the form

$$\Phi_{0lm} \equiv -\frac{r^l}{(1+r)^{2l+1}}\sqrt{4\pi}\,Y_{lm}(\theta, \phi). \tag{2.11}$$

This choice, which is not unique, is motivated by analogy with the usual multipole expansion in that $\Phi_{0lm} \sim r^l Y_{lm}(\theta, \phi)$ near the origin and asymptotically $\Phi_{0lm} \sim r^{-(l+1)}Y_{lm}(\theta, \phi)$ as $r \to \infty$. After some algebra it is easy to show from equation (2.8) that the mass density corresponding to each Φ_{0lm} is

$$\rho_{0lm} = \frac{1}{2\pi}\frac{(2l+1)(l+1)}{r}\frac{r^l}{(1+r)^{2l+3}}\sqrt{4\pi}\,Y_{lm}(\theta, \phi). \tag{2.12}$$

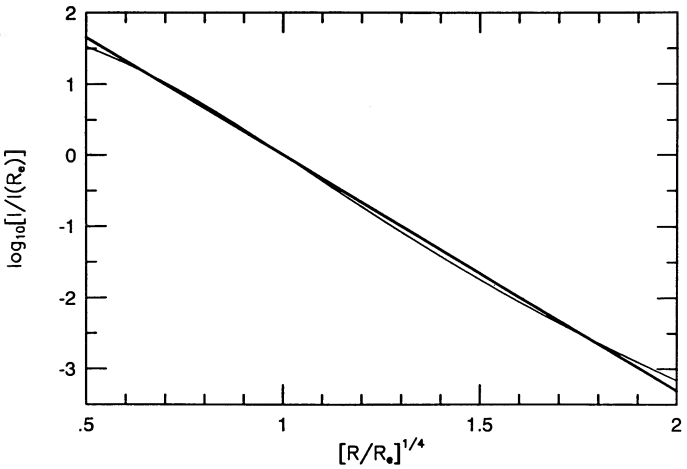

FIG. 1.—Surface brightness profiles for the $R^{1/4}$ law (*thick curve*) and the model analyzed by Hernquist (1990a) (*thin curve*) as a function of $(R/R_e)^{1/4}$. Surface brightness is normalized to its value at R_e, where R_e refers separately to the effective radii of the two models. Maximum difference between the two curves is 35% for $0.05 \leq R/R_e \leq 14.5$.

The arbitrary factor $(4\pi)^{1/2}$ is inserted into both equations (2.11) and (2.12) so that they reduce to the spherical limit defined by equatons (2.9) and (2.10) for $l = m = 0$.

Following CB, write the general terms with $n \neq 0$ in equations (2.6) and (2.7) as

$$\rho_{nlm}(r) \equiv \frac{K_{nl}}{2\pi} \frac{r^l}{r(1+r)^{2l+3}} W_{nl}(\xi) \sqrt{4\pi}\, Y_{lm}(\theta, \phi) , \tag{2.13}$$

$$\Phi_{nlm}(r) \equiv -\frac{r^l}{(1+r)^{2l+1}} W_{nl}(\xi) \sqrt{4\pi}\, Y_{lm}(\theta, \phi) , \tag{2.14}$$

where K_{nl} is a normalization constant and the functions $W_{nl}(\xi)$ include the higher order ($n > 0$) radial dependence. The independent variable ξ is a function solely of r. For $n = 0$ we insist that equations (2.13) and (2.14) reduce to equations (2.11) and (2.12), implying $K_{0l} = (2l + 1)(l + 1)$ and $W_{0l}(\xi) \equiv 1$.

For the present application, it is convenient to select the radial transformation

$$\xi = \frac{r-1}{r+1} . \tag{2.15}$$

Then, the points $r = 0$ and $r = \infty$ correspond to $\xi = -1$ and $\xi = 1$, respectively; i.e., the semi-infinite range $r \in [0, \infty)$ is mapped into the finite interval $\xi \in [-1, 1)$. This change of variables implies

$$r = \frac{1+\xi}{1-\xi} , \tag{2.16}$$

and

$$\frac{d}{dr} = \frac{2}{(1+r)^2} \frac{d}{d\xi} . \tag{2.17}$$

Inserting (2.13) and (2.14) into Poisson's equation (2.8), equations (2.15)–(2.17), it is possible to show that the functions $W_{nl}(\xi)$ satisfy the ordinary differential equation

$$(1-\xi^2) \frac{d^2 W_{nl}}{d\xi^2} - 4(l+1)\xi \frac{dW_{nl}}{d\xi} + 2[K_{nl} - (l+1)(2l+1)] W_{nl} = 0 . \tag{2.18}$$

This can also be written in Sturm-Liouville form

$$\left\{ \frac{1}{(1-\xi^2)^{2l+1}} \frac{d}{d\xi} (1-\xi^2)^{2l+2} \frac{d}{d\xi} + 2[K_{nl} - (l+1)(2l+1)] \right\} W_{nl} = 0 , \tag{2.19}$$

and so the weighting function is $w(\xi) = (1-\xi^2)^{2l+1}$.

From equations (2.18) and (2.19) it is possible to identify the functions $W_{nl}(\xi)$ as various orthogonal polynomials. In particular,

$$W_{nl}(\xi) \equiv c P_n^{(2l+1, 2l+1)}(\xi) , \tag{2.20}$$

where the $P_n^{(\beta,\beta)}$ are Jacobi polynomials and c is an arbitrary constant. When the two upper indices defining the Jacobi polynomials

are equal, as is the case here, they are equivalent to the ultraspherical, or Gegenbauer polynomials, $C_n^{(\alpha)}(\xi)$ (e.g., Szegö 1939; Sommerfeld 1964). The functions $C_n^{(\alpha)}$ obey the differential equation

$$(1-\xi^2)\frac{d^2C_n^{(\alpha)}}{d\xi^2} - (1+2\alpha)\xi\frac{dC_n^{(\alpha)}}{d\xi} + n(n+2\alpha)C_n^{(\alpha)} = 0 . \tag{2.21}$$

Comparing equations (2.18) and (2.21) we infer

$$W_{nl}(\xi) \equiv C_n^{(2l+3/2)}(\xi) , \tag{2.22}$$

and

$$K_{nl} = \tfrac{1}{2}n(n+4l+3) + (l+1)(2l+1) ; \tag{2.23}$$

i.e., $\alpha \equiv 2l + 3/2$ in this case.

Thus, the full basis sets for the density and potential are

$$\rho_{nlm}(\mathbf{r}) = \frac{K_{nl}}{2\pi}\frac{r^l}{r(1+r)^{2l+3}} C_n^{(2l+3/2)}(\xi)\sqrt{4\pi}\, Y_{lm}(\theta,\phi) , \tag{2.24}$$

$$\Phi_{nlm}(\mathbf{r}) = -\frac{r^l}{(1+r)^{2l+1}} C_n^{(2l+3/2)}(\xi)\sqrt{4\pi}\, Y_{lm}(\theta,\phi) , \tag{2.25}$$

where the K_{nl}-values are defined in equation (2.23). Note that both sets of functions are complete. This implies, in particular, that any potential which is everywhere finite can be represented exactly by summing over a sufficiently large number of the Φ_{nlm}. The density distribution corresponding to each basis function is weakly singular at the center. But, the potentials given by equation (2.25) and their gradients tend to finite values at the origin.

It is straightforward to show that the basis functions $\rho_{nlm}(\mathbf{r})$ and $\Phi_{nlm}(\mathbf{r})$ are bi-orthogonal. Write

$$I_{nlm}^{n'l'm'} \equiv \int \rho_{nlm}(\mathbf{r})[\Phi_{n'l'm'}(\mathbf{r})]^* \, d\mathbf{r} . \tag{2.26}$$

Now, the angular integrals in equation (2.26) are just

$$\int_{-1}^{1}\int_0^{2\pi} Y_{lm}(\theta,\phi)Y_{l'm'}^*(\theta,\phi)d(\cos\theta)d\phi = \delta_{l'l}\delta_{m'm} , \tag{2.27}$$

where the Kronicker deltas are defined in the usual way: $\delta_{k'k} = 0$, for $k' \neq k$ and $\delta_{k'k} = 1$, for $k' = k$. Consequently,

$$I_{nlm}^{n'l'm'} = -\frac{K_{nl}}{2\pi} 4\pi\,\delta_{l'l}\delta_{m'm}\int_0^\infty \frac{r^{2l+1}}{(1+r)^{4l+4}} C_n^{(2l+3/2)}(\xi)C_{n'}^{(2l+3/2)}(\xi)dr . \tag{2.28}$$

Transforming the radial integral to one over ξ, using equations (2.15)–(2.17), and taking into account the orthogonality relation of the ultraspherical polynomials:

$$\int_{-1}^{1}(1-\xi^2)^{2l+1}C_n^{(2l+3/2)}(\xi)C_{n'}^{(2l+3/2)}(\xi)d\xi = \frac{\pi 2^{-4l-2}\Gamma(n+4l+3)}{n!(n+2l+3/2)[\Gamma(2l+3/2)]^2}\delta_{n'n} , \tag{2.29}$$

which for $l = 0$ gives $\delta_{n'n}(n+2)(n+1)/(n+3/2)$, so equaton (2.26) can be written as

$$I_{nlm}^{n'l'm'} = I_{nl}\,\delta_{l'l}\,\delta_{m'm}\delta_{n'n} , \tag{2.30}$$

where

$$I_{nl} = -K_{nl}\frac{4\pi}{2^{8l+6}}\frac{\Gamma(n+4l+3)}{n!(n+2l+3/2)[\Gamma(2l+3/2)]^2} , \tag{2.31}$$

which demonstrates that the basis functions are bi-orthogonal.

Given the results of equations (2.28), (2.30), and (2.31) we can now obtain the expansion coefficients, A_{nlm}. Multiply both sides of equation (2.6) by $[\Phi_{n'l'm'}(\mathbf{r})]^*$ and integrate. Then

$$\int \rho(\mathbf{r})[\Phi_{n'l'm'}(\mathbf{r})]^* \, d\mathbf{r} = \sum_{nlm} A_{nlm} I_{nl}\delta_{l'l}\delta_{m'm}\delta_{n'n} = A_{n'l'm'} I_{n'l'} . \tag{2.32}$$

Or, relabeling the indices,

$$A_{nlm} = \frac{1}{I_{nl}}\int \rho(\mathbf{r})[\Phi_{nlm}(\mathbf{r})]^* \, d\mathbf{r} . \tag{2.33}$$

Note, in particular, that the expansion coefficients involve the basis functions for the *potential*, which are finite at the origin.

2.3. *Trivial Examples*

Consider the limit in which the density is spherical, i.e., $\rho(\mathbf{r}) = \rho(r)$. The angular integrals in equation (2.33) then give

$$\int_{-1}^{1}\int_{0}^{2\pi} Y_{lm}^{*}(\theta, \phi)d(\cos\theta)d\phi = \sqrt{4\pi}\,\delta_{l0}\,\delta_{m0}\ . \tag{2.34}$$

After algebra, changing variables from r to ξ, the expansion coefficients are

$$A_{nlm} = \frac{16\pi(n + 3/2)}{(n + 2)(n + 1)[1 + n(n + 3)/2]}\,\delta_{l0}\,\delta_{m0}\int_{-1}^{1}\rho(\xi)\,\frac{(1 + \xi)^2}{(1 - \xi)^3}\,C_n^{(3/2)}(\xi)d\xi\ . \tag{2.35}$$

As a test, consider our initial model given by equation (2.1):

$$\rho(r) = \frac{1}{2\pi}\,\frac{1}{r(1 + r)^3} = \frac{1}{16\pi}\,\frac{(1 - \xi)^4}{1 + \xi}\ . \tag{2.36}$$

The integral over ξ is

$$\frac{1}{16\pi}\int_{-1}^{1}(1 - \xi^2)C_n^{(3/2)}(\xi)d\xi\ . \tag{2.37}$$

Using the fact that $C_0^{(3/2)} = 1$ (see § 3), this integral can be evaluated using equation (2.29):

$$\frac{1}{16\pi}\int_{-1}^{1}(1 - \xi^2)C_0^{(3/2)}C_n^{(3/2)}(\xi)d\xi = \frac{1}{12\pi}\,\delta_{n0}\ . \tag{2.38}$$

Hence,

$$A_{nlm} = \delta_{n0}\,\delta_{l0}\,\delta_{m0}\ , \tag{2.39}$$

as expected.

Next, consider

$$\rho(r) = \frac{3}{4\pi}\,\frac{1}{(1 + r)^4} = \frac{3}{64\pi}\,(1 - \xi)^4\ . \tag{2.40}$$

This model is of interest since it resembles de Zeeuw's perfect ellipsoid (de Zeeuw 1985a, b) and the density is finite at the origin. To evaluate the expansion coefficients, make use of the relation

$$1 - \xi \equiv C_0^{(3/2)}(\xi) - \tfrac{1}{3}C_1^{(3/2)}(\xi)\ . \tag{2.41}$$

Then,

$$A_{nlm} = \frac{3}{4}\,\frac{(n + 3/2)}{(n + 1)(n + 2)[1 + n(n + 3)/2]}\,\delta_{l0}\,\delta_{m0}\int_{-1}^{1}(1 - \xi^2)\left[C_0^{(3/2)} - \frac{1}{3}\,C_1^{(3/2)}\right]C_n^{(3/2)}\,d\xi\ . \tag{2.42}$$

Using the orthogonality relation for the ultraspherical harmonics, equation (2.29), gives

$$A_{nlm} = \tfrac{3}{4}\delta_{n0}\,\delta_{l0}\,\delta_{m0} + \tfrac{1}{12}\delta_{n1}\,\delta_{l0}\,\delta_{m0}\ . \tag{2.43}$$

This can be checked explicitly. From equations (2.23) and (2.24):

$$\rho_{000} = \frac{1}{2\pi}\,\frac{1}{r(1 + r)^3} \tag{2.44}$$

and

$$\rho_{100} = \frac{9}{2\pi}\,\frac{1}{r(1 + r)^3}\,\xi = \frac{9}{2\pi}\,\frac{r - 1}{r(1 + r)^4}\ , \tag{2.45}$$

since $C_0^{(3/2)}(\xi) = 1$ and $C_1^{(3/2)}(\xi) = 3\xi$ (see § 3). So,

$$\frac{3}{4}\,\rho_{000} + \frac{1}{12}\,\rho_{100} = \frac{1}{2\pi}\,\frac{1}{r(1 + r)^3}\left[\frac{3}{4} + \frac{3}{4}\,\frac{r - 1}{r + 1}\right] = \frac{3}{4\pi}\,\frac{1}{(1 + r)^4}\ , \tag{2.46}$$

as it should. This example demonstrates that the basis set defined in equations (2.24) and (2.25) can, in principal, represent even models with nonsingular central densities using only a few terms.

3. IMPLEMENTATION

3.1. *Special Functions*

The functions appearing in the expansions defined by equations (2.24) and (2.25) are straightforward to evaluate. The properties of ultraspherical polynomials are summarized in many standard texts on orthogonal polynomials (e.g., Szegö 1939; Sommerfeld 1964;

CB). The notation adopted here is identical to that of Abramowitz & Stegun (1972). Ultraspherical polynomials are related to Legendre functions by

$$C_n^{(\alpha)}(\xi) = \frac{\Gamma(\alpha + 1/2)\Gamma(2\alpha + n)}{n!\Gamma(2\alpha)} \left[\frac{1}{4}(\xi^2 - 1)\right]^{1/4 - \alpha/2} P_{n+\alpha-1/2}^{1/2-\alpha}(\xi) . \tag{3.1}$$

The term "ultraspherical" derives from the generalization of potential theory to more than three dimensions. That is, if the number of dimensions is $p + 2$, then the potential due to a delta-function source at $\boldsymbol{x}'$ is

$$\frac{1}{|\boldsymbol{x} - \boldsymbol{x}'|} = \sum_{n=0}^{\infty} \frac{r_<^n}{r_>^{n+1}} C_n^{(p/2)}(\cos\gamma) , \tag{3.2}$$

where $r_<$ ($r_>$) is the lesser (greater) of $|\boldsymbol{x}|$ and $|\boldsymbol{x}'|$, γ is the angle between $\boldsymbol{x}$ and $\boldsymbol{x}'$, and $r \equiv |\boldsymbol{x}|$ is the magnitude of the $p + 2$-dimensional vector $\boldsymbol{x}$ (Sommerfeld 1964). For the special case $p = 1$, $C_n^{(1/2)}(\xi) \equiv P_n(\xi)$ and equation (3.2) reduces to the standard expression in three-dimensions (see, e.g., Jackson 1975).

Ultraspherical polynomials are most efficiently computed from the recursion relation

$$(n + 1)C_{n+1}^{(\alpha)}(\xi) = 2(n + \alpha)\xi C_n^{(\alpha)}(\xi) - (n + 2\alpha - 1)C_{n-1}^{(\alpha)}(\xi) . \tag{3.3}$$

which is upwardly stable. Since only the lower index in equation (3.2) varies, suitable starting values are provided by the relations

$$C_0^{(\alpha)}(\xi) = 1 \tag{3.4a}$$

and

$$C_1^{(\alpha)}(\xi) = 2\alpha\xi . \tag{3.4b}$$

The spherical harmonics $Y_{lm}(\theta, \phi)$ are related to Legendre functions by

$$Y_{lm}(\theta, \phi) = \sqrt{\frac{(2l + 1)}{4\pi} \frac{(l + m)!}{(l + m)!}} P_{lm}(\cos\theta) \exp(im\phi) . \tag{3.5}$$

We compute Legendre functions from the recursion relation

$$(l - m)P_{lm}(x) = x(2l - 1)P_{l-1,m}(x) - (1 + m - 1)P_{l-2,m}(x) . \tag{3.6}$$

Only the lower index in equation (3.6) varies, so starting values are provided by

$$P_{mm}(x) = (-1)^m(2m - 1)!!(1 - x^2)^{m/2} \tag{3.7}$$

and

$$P_{m+1,m}(x) = x(2m + 1)P_{mm} . \tag{3.8}$$

3.2. *Evaluation of Expansions*

The basis function expansions introduced in § 2 are complete and can be used to represent any well-behaved potential-density pair. For computational purposes it is convenient to rewrite the expansions in terms of purely real quantities. First, introduce the notation

$$\rho_{nlm}(r) \equiv \tilde{\rho}_{nl}(r)Y_{lm}(\theta, \phi) , \tag{3.9}$$

$$\Phi_{nlm}(r) \equiv \tilde{\Phi}_{nl}(r)Y_{lm}(\theta, \phi) , \tag{3.10}$$

and

$$A_{nlm} \equiv \tilde{A}_{nl} \int \rho(\boldsymbol{r}')\tilde{\Phi}_{nl}(r')Y_{lm}^*(\theta', \phi')d\boldsymbol{r}' . \tag{3.11}$$

By combining terms having the opposite sign of m, the expansion in equations (2.6) and (2.7) can be expressed in terms of real quantities. For convenience, we choose to follow the convention introduced by Bontekoe & van Albada (1987), Bontekoe (1988), and Merritt & Stiavelli (1990).

After some algebra, the density and potential can be written in the forms

$$\rho(r, \theta, \phi) = \sum_{l=0}^{\infty} \sum_{m=0}^{l} P_{lm}(\cos\theta)[A_{lm}(r)\cos m\phi + B_{lm}(r)\sin m\phi] \tag{3.12}$$

and

$$\Phi(r, \theta, \phi) = \sum_{l=0}^{\infty} \sum_{m=0}^{l} P_{lm}(\cos\theta)[C_{lm}(r)\cos m\phi + D_{lm}(r)\sin m\phi] , \tag{3.13}$$

where

$$\begin{pmatrix} A_{lm}(r) \\ B_{lm}(r) \\ C_{lm}(r) \\ D_{lm}(r) \end{pmatrix} = N_{lm} \sum_{n=0}^{\infty} \tilde{A}_{nl} \begin{pmatrix} \tilde{\rho}_{nl}(r) \\ \tilde{\rho}_{nl}(r) \\ \tilde{\Phi}_{nl}(r) \\ \tilde{\Phi}_{nl}(r) \end{pmatrix} \int \rho(r') \tilde{\Phi}_{nl}(r') P_{lm}(\cos\theta') \begin{pmatrix} \cos m\phi' \\ \sin m\phi' \\ \cos m\phi' \\ \sin m\phi' \end{pmatrix} dr' , \tag{3.14}$$

and

$$N_{lm} = \frac{2l+1}{4\pi} (2 - \delta_{m0}) \frac{(l-m)!}{(l+m)!} . \tag{3.15}$$

If the density field consists of a collection of discrete mass-points, i.e.,

$$\rho(r, \theta, \phi) = \sum_k m_k \frac{1}{r_k^2} \delta(r - r_k)\delta(\phi - \phi_k)\delta(\cos\theta - \cos\theta_k) , \tag{3.16}$$

where m_k is the mass of the kth particle, then equation (3.14) becomes

$$\begin{pmatrix} A_{lm}(r) \\ B_{lm}(r) \\ C_{lm}(r) \\ D_{lm}(r) \end{pmatrix} = N_{lm} \sum_{n=0}^{\infty} \tilde{A}_{nl} \begin{pmatrix} \tilde{\rho}_{nl}(r) \\ \tilde{\rho}_{nl}(r) \\ \tilde{\Phi}_{nl}(r) \\ \tilde{\Phi}_{nl}(r) \end{pmatrix} \sum_k m_k \tilde{\Phi}_{nl}(r_k) P_{lm}(\cos\theta_k) \begin{pmatrix} \cos m\phi_k \\ \sin m\phi_k \\ \cos m\phi_k \\ \sin m\phi_k \end{pmatrix} . \tag{3.17}$$

In applications, it may be useful to smooth the density field, perhaps on a grid, before evaluating the integrals leading to equation (3.17).

Accelerations are obtained by differentiating the potential. Since Φ is expressed in spherical coordinates it is expedient to compute spherical accelerations and then calculate Cartesian accelerations from

$$a_x = \sin\theta \cos\phi a_r + \cos\theta \cos\phi a_\theta - \sin\phi a_\phi , \tag{3.18}$$

$$a_y = \sin\theta \sin\phi a_r + \cos\theta \sin\phi a_\theta + \cos\phi a_\phi , \tag{3.19}$$

$$a_z = \cos\theta a_r - \sin\theta a_\theta , \tag{3.20}$$

where (a_r, a_θ, a_ϕ) are the accelerations in spherical coordinates. By taking the gradient of equation (3.13) these accelerations can be written as

$$a_r(r, \theta, \phi) = -\sum_{l=0}^{\infty} \sum_{m=0}^{l} P_{lm}(\cos\theta)[E_{lm}(r) \cos m\phi + F_{lm}(r) \sin m\phi] , \tag{3.21}$$

$$a_\theta(r, \theta, \phi) = -\frac{1}{r} \sum_{l=0}^{\infty} \sum_{m=0}^{l} \frac{dP_{lm}(\cos\theta)}{d\theta} [C_{lm}(r) \cos m\phi + D_{lm}(r) \sin m\phi] , \tag{3.22}$$

$$a_\phi(r, \theta, \phi) = -\frac{1}{r} \sum_{l=0}^{\infty} \sum_{m=0}^{l} \frac{mP_{lm}(\cos\theta)}{\sin\theta} [D_{lm}(r) \cos m\phi - C_{lm}(r) \sin m\phi] , \tag{3.23}$$

where $E_{lm}(r) = dC_{lm}(r)/dr$ and $F_{lm}(r) = dD_{lm}(r)/dr$ and are given by

$$\begin{bmatrix} E_{lm}(r) \\ F_{lm}(r) \end{bmatrix} = N_{lm} \sum_{n=0}^{\infty} \tilde{A}_{nl} \frac{d}{dr} \tilde{\Phi}_{nl}(r) \left[\rho(r') \tilde{\Phi}_{nl}(r') P_{lm}(\cos\theta') \begin{bmatrix} \cos m\phi' \\ \sin m\phi' \end{bmatrix} dr' \right] . \tag{3.24}$$

For a set of discrete point-masses

$$\begin{bmatrix} E_{lm}(r) \\ F_{lm}(r) \end{bmatrix} = N_{lm} \sum_{n=0}^{\infty} \tilde{A}_{nl} \frac{d}{dr} \tilde{\Phi}_{nl}(r) \sum_k m_k \tilde{\Phi}_{nl}(r_k) P_{lm}(\cos\theta_k) \begin{pmatrix} \cos m\phi_k \\ \sin m\phi_k \end{pmatrix} . \tag{3.25}$$

Now,

$$\frac{d}{dr} \tilde{\Phi}_{nl}(r) = -\sqrt{4\pi} \frac{d}{dr} \frac{r^l}{(1+r)^{2l+1}} C_n^{(2l+3/2)}(\xi) . \tag{3.26}$$

Using equation (2.17),

$$\frac{d}{dr} C_n^{(2l+3/2)}(\xi) = \frac{2}{(1+r)^2} \frac{d}{d\xi} C_n^{(2l+3/2)}(\xi) . \tag{3.27}$$

Derivatives of ultraspherical polynomials are given by

$$\frac{d}{d\xi} C_n^{(2l+3/2)}(\xi) = 2(2l + 3/2)C_{n-1}^{(2l+5/2)}(\xi) . \tag{3.28a}$$

[Note from eq. (3.4a) that $dC_0^{(\alpha)}(\xi)/d\xi = 0$. If ultraspherical polynomials are computed using eq. (3.3), then derivatives can be obtained cheaply from

$$2\alpha(1 - \xi^2)C_{n-1}^{(\alpha+1)}(\xi) = (2\alpha + n - 1)C_{n-1}^{(\alpha)}(\xi) - n\xi C_{n-1}^{(\alpha+1)}(\xi) \tag{3.28b}$$

and eq. (3.28a).] Combining equations (3.26)–(3.28a),

$$\frac{d}{dr}\tilde{\Phi}_{nl}(r) = \tilde{\Phi}_{nl}(r)\left[\frac{l}{r} - \frac{2l+1}{1+r} + \frac{4(2l+3/2)}{(1+r)^2}\frac{C_{n-1}^{(2l+5/2)}(\xi)}{C_n^{(2l+3/2)}(\xi)}\right] . \tag{3.29}$$

3.3. *Vectorization*

A considerable gain in performance is realized on computers such as Crays and Convexes through vectorization. The SCF method described here can be fully vectorized, using techniques similar to those for tree and smooth particle hydrodynamics codes (e.g., Hernquist 1990b; Hernquist & Katz 1989). In fact, the innermost sums in equations (3.17) and (3.25) are over the number of particles and so the maximum benefit of vectorization is achieved, since these loops are typically much longer than those over the radial and azimuthal quantum numbers. In essence, this advantage results from the decoupling of the determination of the potential field from the force evaluation and the decomposition of both into N one-body problems (see § 1).

The only subtle point involves vectorizing the evaluation of special functions using recursion relations. Note that relations such as those in equations (3.3) and (3.6) have dependencies that prevent them from being vectorized directly. An alternate strategy is to evaluate the recursion relations for many particles simultaneously so that the inner loop is over particles rather than an index in the recursion relation. In this way, the recursion relations can be fully vectorized at the expense of a modest amount of memory needed to store function evaluations for all the particles.

4. COMPLEMENTARY APPROACHES

It is certainly the case that the formulation discussed here is not unique. For example, the choice for the lowest order terms, ρ_{000} and Φ_{000}, is arbitrary. Those selected here, i.e., equations (2.9) and (2.10), are a reasonable first attempt for modeling galaxies with de Vaucouleurs profiles. However, since the expansion derived here will be less suitable for stellar systems which are badly approximated by an $R^{1/4}$ law, we note below some alternative formulations which may be more appropriate in certain limits.

4.1. *Clutton-Brock*

As we indicated earlier, our method is based on that proposed by CB, who took as his starting point the Plummer model:

$$\rho_{000}(r) = \frac{3}{4\pi}\frac{1}{(1 + r^2)^{5/2}} , \tag{4.1}$$

$$\Phi_{000}(r) = -\frac{1}{(1 + r^2)^{1/2}} . \tag{4.2}$$

Using the same set of steps that led to equations (2.13) and (2.14) gives

$$\rho_{nlm}(r) \equiv \frac{K_{nl}}{4\pi}\frac{r^l}{(1 + r^2)^{l+5/2}} W_{nl}(\xi)\sqrt{4\pi}\, Y_{lm}(\theta, \phi) , \tag{4.3}$$

$$\Phi_{nlm}(r) \equiv -\frac{r^l}{(1 + r^2)^{l+1/2}} W_{nl}(\xi)\sqrt{4\pi}\, Y_{lm}(\theta, \phi) . \tag{4.4}$$

The normalization factor K_{nl} is not necessarily the same as that found earlier. Again, we insist that these functions have the proper limit for $n = 0$, implying that $K_{0l} \equiv (2l + 1)(2l + 3)$ and $W_{0l}(\xi) \equiv 1$.

Now, select the radial transformation

$$\xi \equiv \frac{r^2 - 1}{r^2 + 1} . \tag{4.5}$$

Inserting (4.3) and (4.4) into Poisson's equation (2.8) it is possible to show that the functions $W_{nl}(\xi)$ satisfy

$$(1 - \xi^2)\frac{d^2W_{nl}}{d\xi^2} - (2l + 3)\xi\frac{dW_{nl}}{d\xi} + \frac{1}{4}[K_{nl} - (2l + 1)(2l + 3)]W_{nl} = 0 . \tag{4.6}$$

Comparing equations (4.6) and (2.21) we infer

$$W_{nl}(\xi) \equiv C_n^{(l+1)}(\xi) , \tag{4.7}$$

and

$$K_{nl} \equiv 4n(n + 2l + 2) + (2l + 1)(2l + 3) \; ; \tag{4.8}$$

i.e., $\alpha \equiv l + 1$ in this case. The full basis set is

$$\rho_{nlm}(r) = \frac{K_{nl}}{4\pi} \frac{r^l}{(1 + r^2)^{l+5/2}} C_n^{(l+1)}(\xi) \sqrt{4\pi}\, Y_{lm}(\theta, \phi) \, , \tag{4.9}$$

$$\Phi_{nlm}(r) = -\frac{r^l}{(1 + r^2)^{l+1/2}} C_n^{(l+1)}(\xi) \sqrt{4\pi}\, Y_{lm}(\theta, \phi) \, , \tag{4.10}$$

These expressions are not identical to equations (2.19a, b) in CB owing to differences in labeling ultraspherical polynomials and the different definition of the radial variable ξ.

It is again straightforward to show that the basis functions $\rho_{nlm}(r)$ and $\Phi_{nlm}(r)$ are bi-orthogonal. Evaluating equation (2.26) gives

$$I_{nlm}^{n'l'm'} = I_{nl}\, \delta_{l'l}\, \delta_{m'm}\, \delta_{n'n} \, , \tag{4.11}$$

where

$$I_{nl} = -K_{nl} \frac{\pi}{2^{4l+4}} \frac{(n + 2l + 1)!}{n!(n + l + 1)(l!)^2} \, . \tag{4.12}$$

[Eq. (2.13) in CB apparently contains an error. The factor $(l + 1)!$ appearing in the denominator of the right-hand side of his equation should be $l!$.]

The expansion coefficients, A_{nlm} are again given by equation (2.33), with I_{nl} as in equation (4.12). The detailed implementation of Clutton-Brock's method follows the procedure given in § 3. In particular, equations (3.12)–(3.25) obtain; the only differences are in the exact forms for $\tilde{A}_{nl}$, $\tilde{\rho}_{nl}(r)$, $\tilde{\Phi}_{nl}(r)$, and $d\tilde{\Phi}_{nl}/dr$. These factors are now

$$\tilde{A}_{nl} = -\frac{1}{K_{nl}} \frac{2^{4l+4}}{\pi} \frac{n!(n + l + 1)(l!)^2}{(n + 2l + 1)!} \, , \tag{4.13}$$

$$\tilde{\rho}_{nl}(r) = \frac{K_{nl}}{4\pi} \frac{r^l}{(1 + r^2)^{l+5/2}} C_n^{(l+1)}(\xi) \sqrt{4\pi} \, , \tag{4.14}$$

$$\tilde{\Phi}_{nl}(r) = -\frac{r^l}{(1 + r^2)^{l+1/2}} C_n^{(l+1)}(\xi) \sqrt{4\pi} \, , \tag{4.15}$$

and

$$\frac{d}{dr} \tilde{\Phi}_{nl}(r) = \tilde{\Phi}_{nl}(r) \left[\frac{l}{r} - \frac{(2l + 1)r}{1 + r^2} + \frac{8r(l + 1)}{(1 + r^2)^2} \frac{C_{n-1}^{(l+2)}(\xi)}{C_n^{(l+1)}(\xi)} \right] . \tag{4.16}$$

Note that in equations (4.13–(4.16) K_{nl} is given by equation (4.8) and ξ by equation (4.5).

4.2. *Spherical Bessel Functions*

The basis set constructed in § 2.4 and that described in § 4.1 are best suited for systems that have density profiles similar to those of equations (2.1) or (4.1). A somewhat less specific set involving spherical Bessel functions has been used in a number of analyses of the stability of spheroidal galaxies (e.g., Fridman & Polyachenko 1984; Weinberg 1989). For a finite-sized system of radius R, the appropriate basis functions are (Weinberg 1989)

$$\rho_{nlm} = -\frac{1}{4\pi} \left(\frac{2}{\pi} \right)^{1/2} \left(\frac{\alpha_{nl}}{R} \right)^{5/2} j_l\left(\frac{\alpha_{nl} r}{R} \right) \sqrt{4\pi}\, Y_{lm}(\theta, \phi) \, , \tag{4.17}$$

$$\Phi_{nlm} = \left(\frac{2}{\pi} \right)^{1/2} \left(\frac{\alpha_{nl}}{R} \right)^{1/2} j_l\left(\frac{\alpha_{nl} r}{R} \right) \sqrt{4\pi}\, Y_{lm}(\theta, \phi) \, , \tag{4.18}$$

where the j_l are spherical Bessel functions (e.g., Abramowitz & Stegun 1972) and the α_{nl} are the roots of

$$j_{l-1}(\alpha_{nl}) = 0 \, , \qquad \text{for } l > 0 \tag{4.19a}$$

and

$$\cos(\alpha_{n0}) = 0 \, , \qquad \text{for } l = 0 \, . \tag{4.19b}$$

Equations (4.19a, b) follow from matching the solution to Poisson's equation for $r < R$ with the solution to Laplace's equation for $r > R$ at $r = R$. The functions in equations (4.17) and (4.18) are bi-orthogonal. Writing the normalization condition as in equations (2.30) and (4.11) gives

$$I_{nl} = -\frac{1}{\pi} \alpha_{nl}^3 j_l^2(\alpha_{nl}) \, . \tag{4.20}$$

The notation introduced in § 3 can again be used when implementing this technique. The expansion coefficients, A_{nlm} are given by equation (2.33), with I_{nl} as in equation (4.20). Equations (3.12)–(3.25) obtain for

$$\tilde{A}_{nl} = -\frac{\pi}{\alpha_{nl}^3 j_l^2(\alpha_{nl})}, \tag{4.21}$$

$$\tilde{\rho}_{nl}(r) = -\frac{1}{4\pi}\left(\frac{2}{\pi}\right)^{1/2}\left(\frac{\alpha_{nl}}{R}\right)^{5/2}\sqrt{4\pi}\, j_l\left(\frac{\alpha_{nl} r}{R}\right), \tag{4.22}$$

$$\tilde{\Phi}_{nl}(r) = \left(\frac{2}{\pi}\right)^{1/2}\left(\frac{\alpha_{nl}}{R}\right)^{1/2}\sqrt{4\pi}\, j_l\left(\frac{\alpha_{nl} r}{R}\right), \tag{4.23}$$

and

$$\frac{d}{dr}\tilde{\Phi}_{nl}(r) = \left(\frac{2}{\pi}\right)^{1/2}\sqrt{4\pi}\left(\frac{\alpha_{nl}}{R}\right)^{3/2}\left[j_{l-1}\left(\frac{\alpha_{nl} r}{R}\right) - \frac{l+1}{\alpha_{nl}}\frac{R}{r} j_l\left(\frac{\alpha_{nl} r}{R}\right)\right], \quad \text{for } l > 0 \tag{4.24}$$

$$\frac{d}{dr}\tilde{\Phi}_{n0}(r) = -\left(\frac{2}{\pi}\right)^{1/2}\sqrt{4\pi}\left(\frac{\alpha_{n0}}{R}\right)^{1/2}\frac{1}{r} j_1\left(\frac{\alpha_{n0} r}{R}\right) \quad \text{for } l = 0 . \tag{4.25}$$

A major disadvantage of this basis set is that it is not well-suited for centrally concentrated systems, such as luminous matter in elliptical galaxies. Moreover, Bessel functions take longer to compute than polynomials.

4.3. *Spherical Harmonic Expansions*

For completeness, and to emphasize the differences between previous methods and the one developed here, we choose to describe the "spherical harmonic expansion" technique (e.g., van Albada & van Gorkom 1977; Villumsen 1982; White 1983; McGlynn 1984; Bontekoe & van Albada 1987; Bontekoe 1988; Merritt & Stiavelli 1990). Write the density and potential as in equations (3.12) and (3.13) and insert these into Poisson's equation to give

$$\frac{d^2}{dr^2} C_{lm}(r) + \frac{2}{r}\frac{dC_{lm}(r)}{dr} - \frac{l(l+1)}{r^2} C_{lm}(r) = 4\pi A_{lm}(r) , \tag{4.26}$$

and

$$\frac{d^2}{dr^2} D_{lm}(r) + \frac{2}{r}\frac{dD_{lm}(r)}{dr} - \frac{l(l+1)}{r^2} D_{lm}(r) = 4\pi B_{lm}(r) . \tag{4.27}$$

Rather than expanding C_{lm} and D_{lm} in a radial basis set, as in the SCF method, solve equations (4.26) and (4.27) in closed form using variation of parameters. This gives

$$C_{lm}(r) = -\frac{4\pi}{2l+1} r^{-l-1}\int_0^r ds\, s^{l+2} A_{lm}(s) - \frac{4\pi}{2l+1} r^l \int_r^\infty ds\, s^{1-l} A_{lm}(s) , \tag{4.28}$$

$$D_{lm}(r) = -\frac{4\pi}{2l+1} r^{-l-1}\int_0^r ds\, s^{l+2} B_{lm}(s) - \frac{4\pi}{2l+1} r^l \int_r^\infty ds\, s^{1-l} B_{lm}(s) . \tag{4.29}$$

For a given density field, $\rho(r, \theta, \phi)$, the functions $A_{lm}(r)$ and $B_{lm}(r)$ are determined from the mass distribution by

$$A_{lm}(r) = N_{lm}\int_0^\pi d\theta \sin\theta P_{lm}(\cos\theta)\int_{-\pi}^\pi d\phi \cos m\phi \rho(r, \theta, \phi) , \tag{4.30}$$

$$B_{lm}(r) = N_{lm}\int_0^\pi d\theta \sin\theta P_{lm}(\cos\theta)\int_{-\pi}^\pi d\phi \sin m\phi \rho(r, \theta, \phi) , \tag{4.31}$$

where the N_{lm} are given in equation (3.15). If, for example, $\rho(r)$ is a sum of delta-functions, as in equation (3.16), these become

$$A_{lm}(r) = N_{lm}\sum_k m_k \frac{1}{r_k^2}\delta(r - r_k) P_{lm}(\cos\theta_k)\cos m\phi_k , \tag{4.32}$$

$$B_{lm}(r) = N_{lm}\sum_k m_k \frac{1}{r_k^2}\delta(r - r_k) P_{lm}(\cos\theta_k)\sin m\phi_k . \tag{4.33}$$

The corresponding $C_{lm}(r)$ and $D_{lm}(r)$ are

$$C_{lm}(r) = -(2 - \delta_{m0})\frac{(l-m)!}{(l+m)!}\left[r^{-l-1}\sum_{r_k<r} m_k r_k^l \cos m\phi_k P_{lm}(\cos\theta_k) + r^l \sum_{r_k>r} m_k r_k^{-l-1}\cos m\phi_k P_{lm}(\cos\theta_k)\right], \tag{4.34}$$

$$D_{lm}(r) = -(2 - \delta_{m0})\frac{(l-m)!}{(l+m)!}\left[r^{-l-1}\sum_{r_k<r} m_k r_k^l \sin m\phi_k P_{lm}(\cos\theta_k) + r^l \sum_{r_k>r} m_k r_k^{-l-1}\sin m\phi_k P_{lm}(\cos\theta_k)\right]. \tag{4.35}$$

In spherical coordinates, the components of acceleration are as in equations (3.21)–(3.23). Writing

$$C_{lm}(r) = C_{lm}^{(1)}(r) + C_{lm}^{(2)}(r) , \tag{4.36}$$

where $C_{lm}^{(1)}(r)$ and $C_{lm}^{(2)}(r)$ are the two terms defining $C_{lm}(r)$ above, then it is trivial to show that

$$E_{lm}(r) = -(l+1)\frac{C_{lm}^{(1)}(r)}{r} + l\frac{C_{lm}^{(2)}(r)}{r} . \tag{4.37}$$

Similarly,

$$F_{lm}(r) = -(l+1)\frac{D_{lm}^{(1)}(r)}{r} + l\frac{D_{lm}^{(2)}(r)}{r} , \tag{4.38}$$

where $D_{lm}^{(1)}(r)$ and $D_{lm}^{(2)}(r)$ are the two terms defining $D_{lm}(r)$.

The principal difference between this approach and SCF methods can readily be discerned from equations (4.34)–(4.35). Unlike SCF algorithms, the potential depends on the relative coordinates of particles. For example, the potential of particle i depends implicitly on the relative values of r_i and r_k ($k \neq i$) owing to the summation indices in equations (4.34) and (4.35). This "spherical harmonic expansion" method is, in fact, a hybrid N-body-basis set technique. Of course, it would be possible to expand the radial part of the potential in terms of an efficient set of basis functions as in the original work of Ostriker & Mark (1968) and earlier in this paper (§ 2) and then determine coefficients by integrating over $C_{lm}(r)$ and $D_{lm}(r)$, as given by equations (4.34) and (4.35).

Note that the force between two particles in the spherical expansion method diverges as they pass by one another in the radial direction. The particles interact with one another in an N-body sense as if they are portions of spherical shells (e.g., McGlynn 1984), as can be inferred from the expression above for the density (eqs. [4.32] and [4.33]). This divergence can be prevented by introducing softening, as in other N-body codes. (Note, however, that softening ameliorates relaxation effects relatively weakly in three dimensions.) This can be accomplished either by smoothing the density on a grid (van Albada & van Gorkom 1977) or by introducing an explicit softening into the equations of motion (Villumsen 1982). One example of the latter is due to White (1983) who writes

$$C_{lm}(r) = -(2-\delta_{m0})\frac{(l-m)!}{(l+m)!}\left[(r^2+\epsilon^2)^{-(l+1)/2}\sum_{r_k<r} m_k r_k^l \cos m\phi_k P_{lm}(\cos\theta_k) + r^l \sum_{r_k>r} m_k (r_k^2+\epsilon^2)^{-(l+1)/2} \cos m\phi_k P_{lm}(\cos\theta_k)\right], \tag{4.39}$$

and

$$D_{lm}(r) = -(2-\delta_{m0})\frac{(l-m)!}{(l+m)!}\left[(r^2+\epsilon^2)^{-(l+1)/2}\sum_{r_k<r} m_k r_k^l \sin m\phi_k P_{lm}(\cos\theta_k) + r^l \sum_{r_k>r} m_k (r_k^2+\epsilon^2)^{-(l+1)/2} \sin m\phi_k P_{lm}(\cos\theta_k)\right], \tag{4.40}$$

where ϵ is the softening length. To prevent numerical instability, it is advisable to set $\epsilon^2 \rightarrow \epsilon^2/2$ for $l = m = 0$ (White 1983). The radial acceleration is obtained by differentiating equations (4.39) and (4.40).

5. TESTS

5.1. *Code*

We have developed and implemented a code to evolve Monte Carlo realizations of the density field with the various methods described in §§ 2.1 and 4.1–4.3. This code is fully vectorized using techniques like those summarized in § 3.3. Time integration is performed using a time-centered leapfrog algorithm to maintain time reversibility (e.g., Press et al. 1986).

The cpu cost of the SCF method scales with particle number as $\sim O(N)$. The "spherical harmonic expansion" technique discussed in § 4.3 scales as $\sim O(N \log N)$ since this approach requires that the particles be sorted in radius. For $N = 10^4$, retaining terms up to $n = 6$ and $l = 4$ in equations (2.6) and (2.7), the force calculation algorithm presented here requires approximately 0.5 cpu seconds per step on either a Cray Y-MP or a Cray 2. Since the cpu cost is linear in N, runs with $N = 10^6$ would require less than 1 cpu minute per step. Given sufficient resources, runs with $N \sim 10^7$–10^8 are not out of the question, especially if somewhat lower radial and angular resolution is needed.

Evidently, vectorization is quite efficient for the algorithm discussed here. A run with the same parameters as above requires approximately 30 cpu seconds per step on a Sun Sparcstation-2, and is consequently ≈ 60 times slower than on either a Cray Y-MP or Cray 2. Adopting the Linpack benchmark of 3.3 Mflops for the Sparcstation-2 (e.g., Dongarra 1991), these estimates imply that the SCF method achieves nearly 200 Mflops on a single-processor Cray. (The runs on the Sparcstation-2 were done using the compile options -O3-cg89, which represent the highest level of optimization available.)

The SCF method conserves the total energy of the system exactly, aside from time-integration errors and round-off effects. Total angular momentum is conserved to round-off accuracy. The conservation of total linear momentum is, however, weakly violated.

5.2. *Static Tests*

From a computational standpoint the method presented here is useful only to the extent that the basis function expansions provide a good approximation to systems of interest with only a few terms. It is anticipated that our particular basis set will be best

suited for modeling perturbations about the exact spherical state specified by equations (2.1) and (2.2). As an extreme test of the method's ability to represent deviations from this density profile, we calculate expansion coefficients for several well-known potential-density pairs to give some indication of how many terms will typically be needed in dynamical simulations.

5.2.1. *Radial Convergence of Expansion*

Consider the limit in which the density field is spherical, i.e., $\rho(\mathbf{r}) = \rho(r)$. Then, the expansion coefficients are given by equation (2.35). Except in special cases, e.g., those in § 2.3, the integral in equation (2.35) must be done numerically. We have done this for six commonly used models: (1) that in equation (2.1) with arbitrary a, (2) the spherical limit of the perfect ellipsoid

$$\rho(r) = \frac{a}{\pi^2}\frac{1}{(a^2 + r^2)^2}, \tag{5.1}$$

(3) Plummer's model (eq. [4.1]), (4) the isochrone (e.g., Binney & Tremaine 1987), (5) the $R^{1/4}$ law (e.g., Young 1976), and (6) King truncated isothermals (King 1966) with various ratio of tidal to core radii.

Values of the expansion coefficients, A_{n00} are shown in Figure 2 for these models. The expansion coefficients for model (1) with $a = 2$ decline exponentially with n. This is reassuring, since if one were to use the expansion to fit, say, the results of a numerical experiment or even an observation, the fact that the basis expansions were performed assuming $a = 1$ is not a limitation. For most of the other models, the coefficients also decline exponentially with increasing n but somewhat more slowly. Exceptions are the $R^{1/4}$ law (5) and King profile (6), whose coefficients decay more like a power law. This is in part due to the fact that these density distributions have an exponential tail at large radii whereas the basis functions used here have a power-law character asymptotically. The King model illustrated in Figure 2 has a concentration parameter $c = \log_{10}(r_t/r_0) = 1.4833$, where r_t/r_0 is the ratio of tidal to King radius (e.g., Binney & Tremaine 1987). Results for other values of c are qualitatively similar to that shown in Figure 2.

The results in Figure 2 suggest that $\lesssim 1\%$ accuracy can be achieved with $\lesssim 5$–6 radial basis functions. It is also clear that, although the ρ_{000} term diverges at $r = 0$, a good representation of models with density cores is possible retaining only a few terms (see also § 2.3), since the coefficients are computed using the potential expansion, which is finite at the origin. We discuss in § 6 the ability of the adopted expansion to model a typical galaxy with a flat rotation curve.

The steep decline of the A_{n00} shown in Figure 2 provides a global measure of the accuracy of the expansion. Figure 3 shows a more local estimate of the inaccuracies made by truncating the expansions at a maximum value of n, $n_{\max}$, where the radial acceleration in a spherical perfect model, a_r, (eq. [5.1]) is compared to its estimate computed from equation (3.21). The acceleration converges rapidly to its analytical value for large r. The large deviations seen at small radii result from the fact that the density in equation (5.1) has a core while that in equation (2.1) does not. (Note, however, that the acceleration does converge to its exact value at all r for sufficiently large $n_{\max}$, as ensured by the completeness of the basis functions.) Though somewhat alarming, these differences are probably not significant from a dynamical point of view. For $n_{\max} = 6$, the acceleration is computed to better than 1% accuracy over 99.4% the mass of the perfect model. For $n_{\max} = 10$ this fraction rises to 99.998%. The fact that the acceleration is not necessarily well-represented for this residual mass is not important since $a_r \to 0$ as $r \to 0$.

Figure 3 suggests that $n_{\max} \lesssim 10$ will be adequate in most cases, provided that the actual density profile is not terribly different from the lowest order one in the basis set derived in this paper. Naturally, this claim should be checked by varying $n_{\max}$ to determine whether or not a given solution has converged.

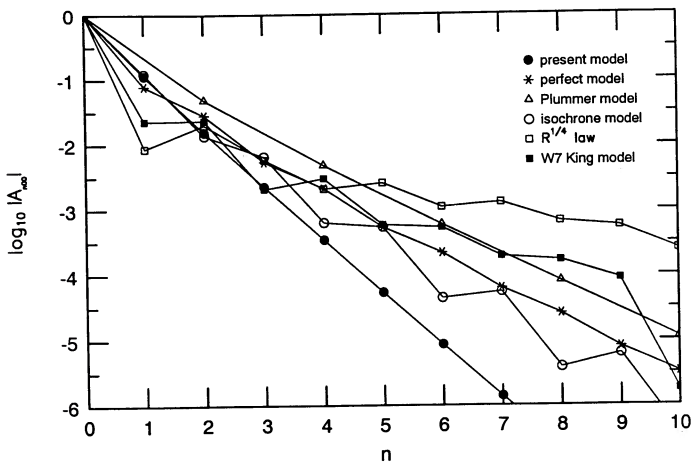

FIG. 2

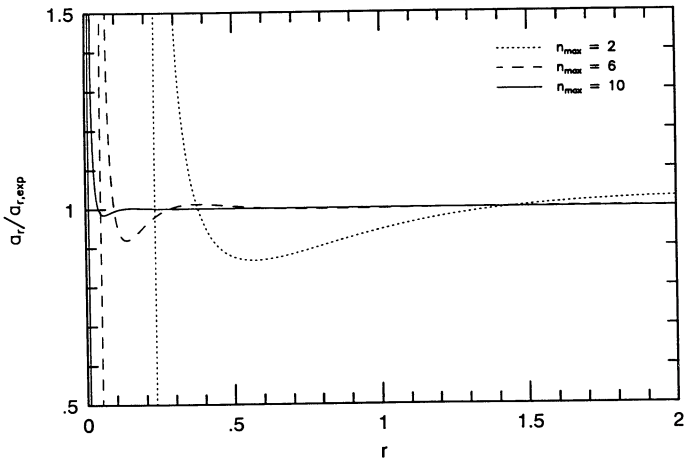

FIG. 3

FIG. 2.—Expansion coefficients in eqs. (2.6) and (2.7) for spherical models using the basis set defined in eqs. (2.24) and (2.25). Shown are coefficients for the model studied by Hernquist (1990a; eq. [2.1]) with scale length $a = 2$ (*filled circles*, [1]), the perfect spherical model (de Zeeuw 1985a, b; eq. [5.1]; *asterisks*, [2]) with unit scale length, Plummer's model with unit scale length (*triangles*, [3]), the isochrone model with unit scale length (*open circles*, [4]), the $R^{1/4}$ law with $R_e = 2$ (*open squares*, [5]), and a King model with concentration parameter $c = 1.4833$ (*filled squares*, [6]). Values of A_{n00} are normalized to A_{000}.

FIG. 3.—Radial acceleration in a perfect sphere (eq. [5.1]) with unit scale length, divided by its value calculated from the basis function expansion derived in this paper, as a function of radius. The three curves show the effect of truncating the expansion at a given value of $n_{\max}$, the index of the maximum radial term retained. Divergence as $r \to 0$ due to fact that $a_r \to 0$ in the exact solution.

5.2.2. *Angular Convergence of Expansion*

Next, consider models that are axisymmetric about the z-axis, i.e., $\rho(\mathbf{r}) = \rho(R, z)$, where $R = (x^2 + y^2)^{1/2}$ is the cylindrical radius. It is then possible to show that

$$A_{nlm} = \frac{2^{2l+3} n!(n + 2l + 3/2)\sqrt{2l + 1}\,\pi[(4l + 1)!!]^2}{[(l + 1)(2l + 1) + n(n + 4l + 3)/2](n + 4l + 2)!}\,\delta_{m0} \int_{-1}^{1}\int_{-1}^{1} \rho(r, \theta)(1 + \xi)^{l+2}(1 - \xi)^{l-3} C_n^{(2l+3/2)}(\xi) P_l(\cos\theta) d\xi\, d(\cos\theta)\,. \tag{5.2}$$

Let us compute the A_{nlm} for the axisymmetric generalization of equation (2.1):

$$\rho(r, \theta) = \frac{M}{2\pi a^2 c}\,\frac{1}{\mu(1 + \mu)^3}\,, \tag{5.3}$$

where

$$\mu^2 = \frac{x^2}{a^2} + \frac{y^2}{a^2} + \frac{z^2}{c^2} = \frac{r^2}{a^2 c^2}\,[c^2 + (a^2 - c^2)\cos^2\theta]\,. \tag{5.4}$$

Note that the mass enclosed within a given ellipsoidal radius, μ is

$$M(\mu) = M\,\frac{\mu^2}{(1 + \mu)^2}\,. \tag{5.5}$$

Since $\rho(r, \theta)$ is an even function of $\cos\theta$, terms involving odd l are identically zero. The A_{nlm} cannot be calculated analytically for general a and c, and the integrals in equation (5.2) must be done numerically.

Figure 4 shows expansion coefficients for this density profile with $M = 1$, $a = 1$, and $c = 0.5$. For a given l, A_{nl0} declines roughly exponentially with n, as found previously for the spherical version of this model (Fig. 2). Figure 4 indicates that the expansion coefficients increase in magnitude with l for a fixed value of n. This does not imply that the expansions diverge since the basis function decrease with l at a given position.

The radial acceleration, normalized to its exact value, is given in Figure 5 for the same model used in Figure 4. The acceleration shown here is measured along the x-axis. Other directions give comparable results. The polar acceleration, a_θ, and magnitude of the acceleration exhibit similar departures from the corresponding exact values. For $n_{max} = 6$ and $l_{max} = 2$ the discrepancy is less than 1% except within the inner regions containing $\sim 5\%$ of the mass. Substantial improvement is achieved by increasing l_{max} to 6 and then n_{max} to 10. For $n_{max} = 10$ and $l_{max} = 6$ the deviation is $\lesssim 0.2\%$ except within the inner 0.01% of the mass where the errors are $\sim 1\%$. Unless unusually high accuracy is required, $l_{max} \lesssim 6$ should suffice, at least for models with axis ratios $\approx 2{:}1$.

5.3. *Dynamical Tests*

To assess the severity of relaxation effects in the SCF method, we adopt the technique employed by Hernquist & Barnes (1990). In the ideal collisionless limit, energies and angular momenta of individual particles are strictly conserved. Owing to discreteness noise for finite N, particle energies and angular momenta are not conserved in Monte Carlo integrations and the degree to which these conservation laws are violated provides a convenient gauge of relaxation effects.

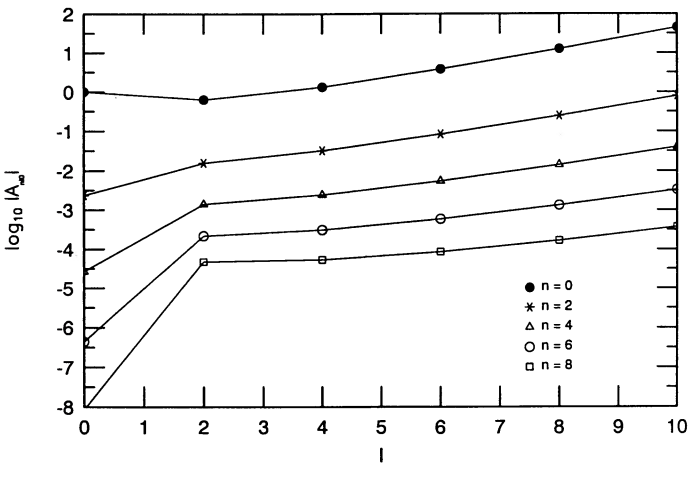

FIG. 4

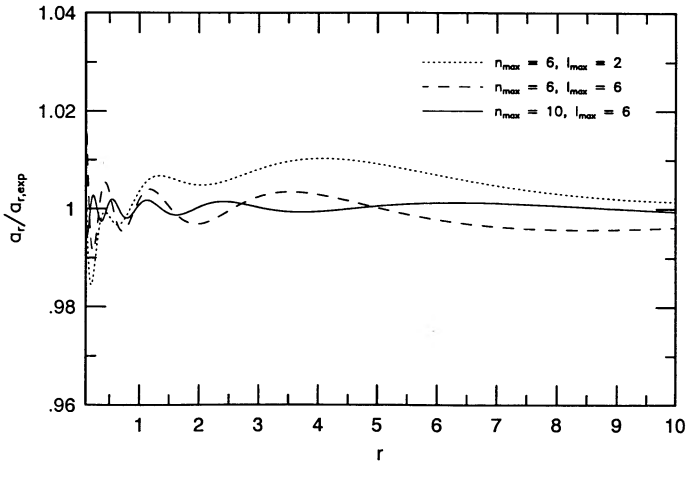

FIG. 5

FIG. 4.—Expansion coefficients in eqs. (2.6) and (2.7) for an axisymmetric model of the form given in eq. (5.3) using the basis set defined in eqs. (2.24) and (2.25). The axis ratio is $a{:}c = 1{:}0.5$ and the model has unit mass. Values of A_{nl0} are normalized to A_{000}.

FIG. 5.—Radial acceleration in an axisymmetric generalization of the model studied by Hernquist (1990a; eq. [2.1]) with scale lengths $a = 1$ and $c = 0.5$, divided by its value calculated from the basis function expansion derived in this paper, as a function of radius. The three curves show the effect of truncating the expansion at a given value of l_{max}, the index of the maximum angular term retained and n_{max}, the index of the maximum radial term retained.

We have performed a large number of calculations in which the energies and angular momenta of individual particles were monitored. A representative subset of the results is presented below. Monte Carlo realizations of the density field given by equation (2.1) were generated from the exact distribution function of this model (Hernquist 1990a). The characteristic dynamical time is (e.g., Binney & Tremaine 1987)

$$t_{\rm dyn} \equiv \sqrt{\frac{3\pi}{16G\bar{\rho}}}\,, \tag{5.6}$$

where

$$\bar{\rho} \equiv \frac{M(r)}{4\pi r^3/3} \tag{5.7}$$

is the mean density within a given radius, r. For the model of equation (2.1),

$$\bar{\rho} = \frac{3}{4\pi}\,\frac{M}{r}\,\frac{1}{(r+a)^2}\,. \tag{5.8}$$

In a system of units with $G = 1$, $M = 1$, and $a = 1$ equations (5.6) and (5.8) imply that

$$t_{\rm dyn} = \frac{\pi}{2}\,(1+r)r^{1/2}\,. \tag{5.9}$$

At the half-mass radius, $r_{1/2} = 1 + 2^{1/2}$, the dynamical time is

$$t_{\rm dyn,\,1/2} = \frac{\sqrt{2}}{2}\,\pi(1+\sqrt{2})^{3/2} \approx 8.333\,. \tag{5.10}$$

For ease of comparison with less efficient methods, we performed runs mainly with $N = 10^4$ particles. (Extrapolation to higher N is straightforward.) Equilibrium models were typically integrated from $t = 0$ to $t = 200$ and particle energies and angular momenta were recorded at various times. Figure 6 shows the change in energy of the particles in one of the runs made with the SCF method described in § 2, as a function of the binding energy per unit mass. The change in energy was measured from $t = 100$ to $t = 200$ to eliminate initial transients (Hernquist & Barnes 1990). Figure 7 shows a similar plot obtained using the spherical harmonic expansion technique of § 4.3. Both the calculations in Figures 6 and 7 were performed using a time-step $\Delta t = 0.01$, implying a total of ≈ 833 steps per half-mass dynamical time. The total system energy was conserved to 5 significant figures. In both cases, terms up to quadrupole order were included in the angular expansions ($l_{\rm max} = 2$) and the SCF run was performed with $n_{\rm max} = 0$. A similar simulation made with a hierarchical tree-code (Hernquist 1987) is shown in Figure 8. Owing to the much greater cpu costs of the tree-code, a time-step $\Delta t = 0.05$ was used and the system energy was conserved to only 3 significant figures. Forces were computed with a tolerance parameter $\theta_{\rm tree} = 0.7$, including terms up to quadrupole order. In the runs with the spherical harmonic expansion and the tree-code, a softening length $\epsilon = 0.2$ was chosen, which is approximately the mean interparticle separation at the half-mass radius with 10^4 particles. In Figures 6–8, the change in energy of each particle is measured relative to the binding energy of each particle at $t = 100$.

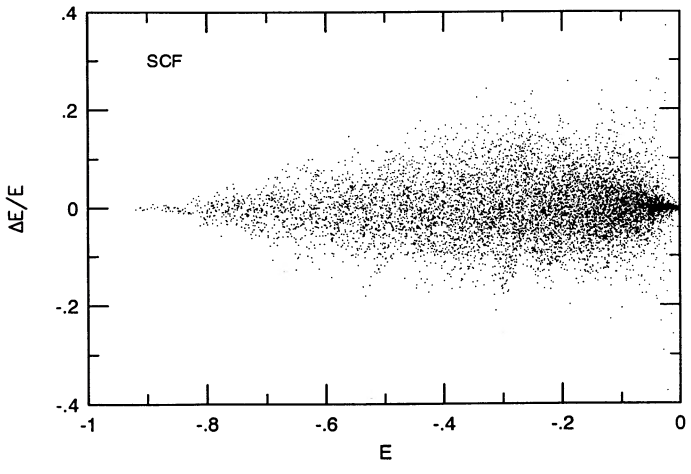

FIG. 6

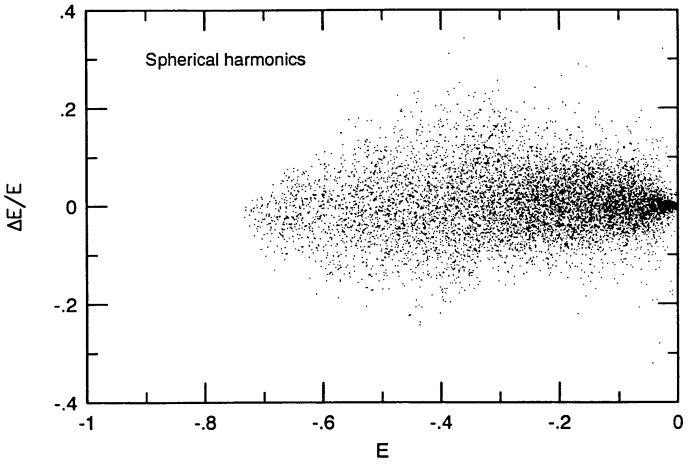

FIG. 7

FIG. 6.—Changes in energies of individual particles in a model of the type specified by eqs. (2.1) and (2.2) between $t = 100$ and $t = 200$, as a function of the binding energy per unit mass at $t = 100$ (units such that half-mass dynamical time, eq. [5.6], is 8.333). Energy differences are measured relative to each particles' binding energy at $t = 100$. Forces were calculated using the SCF method derived in § 2. A total of $N = 10{,}000$ particles were used and the time step was $\Delta t = 0.01$. Note the presence of tightly bound particles ($E < -0.8$) owing to the lack of softening in the SCF method.

FIG. 7.—Same as in Fig. 6, but with forces computed using the spherical harmonic expansion technique described in § 4.5. A softening length $\epsilon = 0.2$ was used.

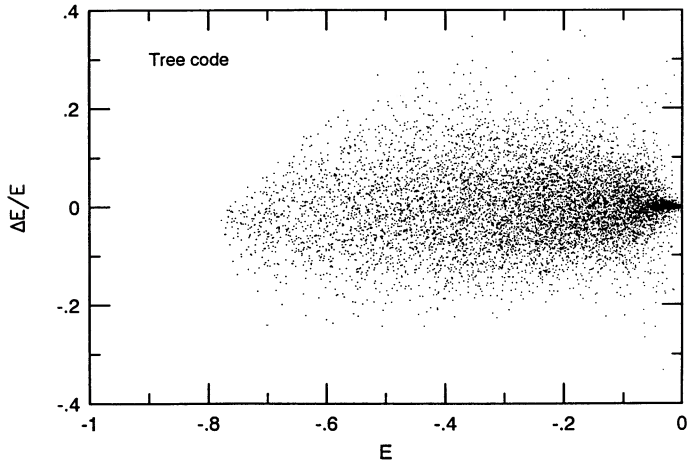

FIG. 8.—Same as in Fig. 6, but with forces computed using a hierarchical tree-code. A softening length $\epsilon = 0.2$ was used and the time step was $\Delta t = 0.05$.

To quantify the effects of relaxation implied by Figures 6–8, we measure the standard deviation

$$\sigma \equiv \left[\frac{1}{N-1}\sum_{k=1}^{N}\left(\frac{\Delta E_k}{E_k} - \overline{\Delta E}\right)^2\right]^{1/2} \tag{5.11}$$

and absolute deviation

$$A \equiv \frac{1}{N}\sum_{k=1}^{N}\left|\frac{\Delta E_k}{E_k} - \overline{\Delta E}\right| \tag{5.12}$$

for each distribution, where

$$\overline{\Delta E} \equiv \frac{1}{N}\sum_{k=1}^{N}\frac{\Delta E_k}{E_k} \tag{5.13}$$

is the mean change in energy per particle. Values of σ, A, and $\overline{\Delta E}$ for the three runs in Figures 6–8 are given in Table 1, along with those for another calculation in which the particles were integrated in the fixed, non-self-consistent field specified by equation (2.2) and four others made with the SCF and spherical harmonic expansion (here, and Table 2 referred to as SHE) methods for $l_{max} = 0$ and $l_{max} = 4$.

TABLE 1

FRACTIONAL CHANGE IN PARTICLE ENERGIES IN VARIOUS RUNS

Run	Method	σ	A	σ/A	$\overline{\Delta E}$
1.....	Fixed Field	7.12E−5	3.23E−6	...	−7.61E−7
2.....	SCF, $l_{max} = 0$	5.92E−3	3.73E−3	1.59	−3.82E−4
3.....	SCF, $l_{max} = 2$	5.62E−2	4.06E−2	1.38	−4.39E−4
4.....	SCF, $l_{max} = 4$	5.66E−2	4.09E−2	1.39	−1.35E−3
5.....	SHE, $l_{max} = 0$	2.94E−2	1.90E−2	1.54	−4.10E−6
6.....	SHE, $l_{max} = 2$	6.05E−2	4.34E−2	1.40	2.69E−3
7.....	SHE, $l_{max} = 4$	6.89E−2	5.18E−2	1.33	1.14E−3
8.....	Tree-code	7.11E−2	5.09E−2	1.40	−1.93E−3

TABLE 2

FRACTIONAL CHANGE IN L_z FOR PARTICLES IN VARIOUS RUNS

Run	Method	σ	A	σ/A	$\overline{\Delta L_z}$
1.....	Fixed Field	2.12E−10	5.85E−12	...	−2.50E−12
2.....	SCF, $l_{max} = 0$	2.12E−10	5.82E−12	...	−2.48E−12
3.....	SCF, $l_{max} = 2$	8.18E−2	5.78E−2	1.42	−4.51E−10
4.....	SCF, $l_{max} = 4$	8.40E−2	5.89E−2	1.43	3.53E−10
5.....	SHE, $l_{max} = 0$	2.10E−10	5.45E−12	...	−2.48E−12
6.....	SHE, $l_{max} = 2$	1.25E−1	9.28E−2	1.35	3.14E−10
7.....	SHE, $l_{max} = 4$	2.15E−1	1.64E−1	1.31	6.09E−10
8.....	Tree-code	1.40E−1	1.07E−1	1.32	−5.40E−5

Several conclusions can be drawn from Figures 6–8 and Table 1. First, σ and A for the run in the fixed potential are much smaller than any of the others, as expected, so time-integration and round-off errors are negligible. Second, values of σ and A for the SCF method, the spherical harmonic expansion technique, and the tree-code are roughly the same, on average, for $l_{\max} > 0$. This similarity between the tree-code and the spherical harmonic expansion technique was noted previously by Hernquist & Barnes (1990). The fact that the SCF technique is not significantly different from either of these other algorithms implies that it suffers from similar levels of relaxation, contrary to the claim made by Allen et al. (1990).

Figure 6, in comparison with Figures 7 and 8, shows that the SCF method retains tightly-bound particles more readily than do N-body schemes. This is due to the lack of softening in the SCF code and implies that there are no intrinsic limitations on local spatial resolution aside from particle discreteness. Thus, the SCF method may be capable of resolving steeper density gradients than direct N-body techniques. For example, one can explore subregions at high resolution with the SCF method by populating them with particles having a mass spectrum. The use of particles with different masses in direct N-body codes does not, by itself, improve resolution locally unless, in addition, one incorporates a scheme allowing the softening length to vary from one particle to another.

To further determine the nature of the lack of energy conservation of each particle in the SCF method, we ran an additional model up to $t = 1000$ and determined σ, A, and $\overline{\Delta E}$ as a function of the time interval between measurements; results are given in Figure 9. Note that both σ and A are well-fitted by a time-dependence proportional to $\delta t^{1/2}$, which is characteristic of diffusive phenomena. It is possible to use these fits to obtain a rough estimate of the energy relaxation time. From the values of A and the appropriate scaling with particle number N (Hernquist & Barnes 1990),

$$A \sim 0.01\left(\frac{\delta t}{t_{\rm dyn,\,1/2}}\right)^{1/2}\left(\frac{N}{10^4}\right)^{-1/2}, \tag{5.14}$$

where $t_{\rm dyn,\,1/2} \approx 8.333$ is the half mass dynamical time of the model. To the extent that the various methods used to obtain A give similar results, equation (5.14) is only weakly dependent on the number of terms retained in the basis function expansions. Defining the energy relaxation time, t_r, to be the time for which $A \sim 1$ implies

$$\frac{t_r}{t_{\rm dyn,\,1/2}} \sim 10^4\left(\frac{N}{10^4}\right). \tag{5.15}$$

Certainly, this estimate appears quite impressive since it suggests that relaxation effects will be modest for hundreds of dynamical times even with N as small as 10^4. However, we believe that this inference is extremely deceptive since orbital diffusion can modify the phase-space structure of models significantly even if A is much less than one.

Quantifying the diffusion of particles' angular momenta, $\boldsymbol{L}$, is complicated by the fact that many particles in isotropic models like those considered here have $|\boldsymbol{L}| \approx 0$. In such cases, even a small absolute change in $\boldsymbol{L}_i$ for some particle i will yield a large fractional error when measured relative to $\boldsymbol{L}_i$. To circumvent this problem, we measure changes in angular momenta relative to the mean absolute value of $\boldsymbol{L}$, averaged over all particles, $\langle|\boldsymbol{L}|\rangle$, defined by

$$\langle|\boldsymbol{L}|\rangle = \frac{1}{N}\sum_{k=1}^{N}|\boldsymbol{L}_k|\,. \tag{5.16}$$

Figures 10–12 show changes in L_x between $t = 100$ and $t = 200$ for the particles in the runs used to generate Figures 6–8, relative to $\langle|L_x|\rangle$ at $t = 100$. (Results for the other components of $\boldsymbol{L}$ are quantitatively similar.) Moments of these distributions are given in Table 2, along with those for the other five runs listed in Table 1. The moments shown in Table 2 measure changes in angular momentum relative to $\langle|L_x|\rangle$.

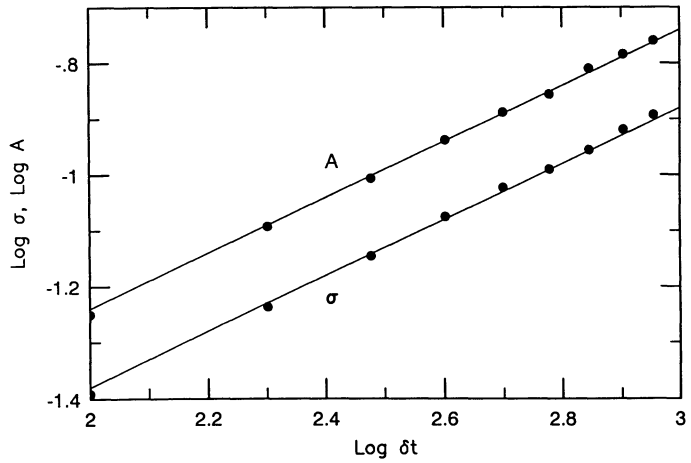

FIG. 9.—Logarithm of standard deviation and absolute deviation of particle energies for a longer version of the run in Fig. 6, as a function of the logarithm of the separation in measurement times, δt. Filled circles are measured values, while solid lines have slope $\frac{1}{2}$. Upper points are standard deviation, σ, and lower points are absolute deviation, A.

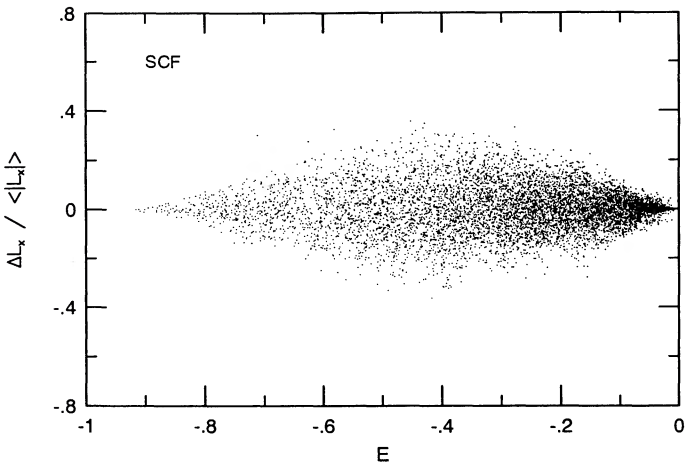

FIG. 10

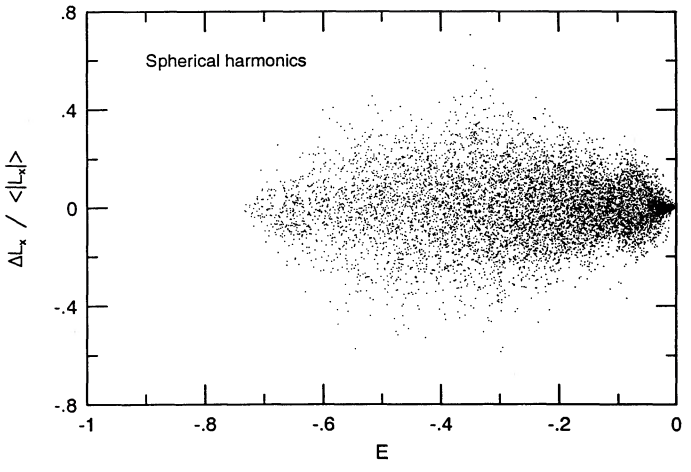

FIG. 11

FIG. 10.—Changes in the x-component of angular momentum of individual particles in the model used to obtain Fig. 6 between $t = 100$ and $t = 200$, as a function of the binding energy per unit mass at $t = 100$. Forces were calculated using the SCF method derived in § 2. Note the presence of tightly bound particles ($E < -0.8$) owing to the lack of softening in the SCF method.

FIG. 11.—Same as in Fig. 10, but with forces computed using the spherical harmonic expansion technique described in § 4.5. Other parameters are as in Fig. 7.

The results summarized in Figures 10–12 and Table 2 support our earlier claim that the various methods suffer from comparable levels of nonconservation of integrals of motion. Comparing the entries in Table 2 for the SCF method with $l_{max} = 2$, the spherical harmonic expansion technique with $l_{max} = 2$, and a tree-code suggest that particles' angular momenta are conserved to similar accuracy in these various methods, at least to within a factor ~ 2. In the limit $l_{max} = 0$ both the SCF and spherical harmonic expansion methods conserve $\boldsymbol{L}$ exactly since forces are then perfectly radial.

The results in Tables 1 and 2 imply that energy and angular momentum conservation are violated to similar degrees. This is to some extent an artifact of the procedure we employ to quantify changes in particles' angular momenta. In fact, many of those particles with total angular momentum near zero experienced quite large changes relative to their individual angular momenta. In other words, orbits with small total angular momenta tend to be destroyed at rates much higher than one might infer from the entries in Table 2. Clearly, this inference has serious implications for any attempt to quantify orbital structure of computer models obtained by N-body simulation.

For a Gaussian probability function, $\sigma/A = (\pi/2)^{1/2} \approx 1.253$, while for an exponential distribution, $\sigma/A = 2^{1/2} \approx 1.414$. It is interesting that the values of σ/A listed in Tables 1 and 2 are closer to the result for an exponential distribution than a Gaussian one. If the particle accelerations are experiencing fluctuations of a Gaussian character, we might expect particle velocities to exhibit similar fluctuations. A variation in velocity, δv, will, to leading order, give rise to perturbations in energy, $\delta E \propto v\,\delta v$, implying that changes in particle energies will be distributed according to an exponential profile. Naturally, this argument is not rigorous and, in fact, the values of σ/A show considerable scatter.

It is perhaps surprising that the SCF method is similar to the others tested here in terms of its relaxation properties, in spite of its intrinsic mean-field character. The reason for this behavior can be deduced from Figure 13, which shows the time-dependence of the

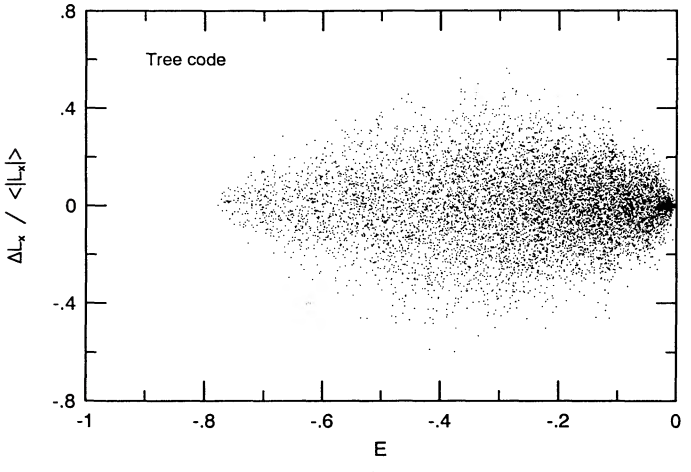

FIG. 12

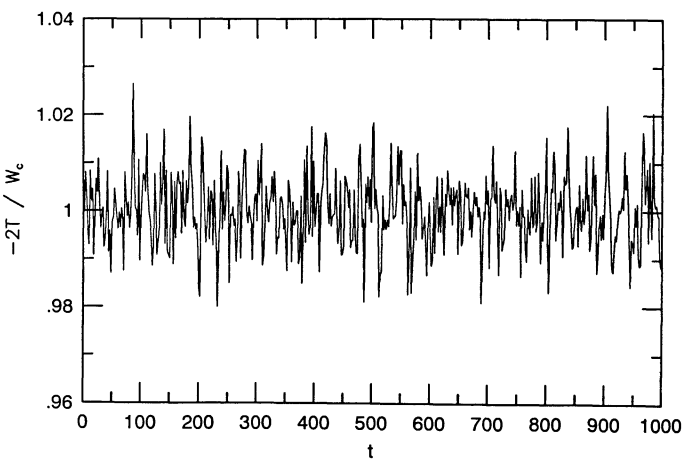

FIG. 13

FIG. 12.—Same as in Fig. 10, but with forces computed using a hierarchical tree-code. Other parameters are as in Fig. 8.

FIG. 13.—Minus twice the kinetic energy divided by the trace of the potential energy tensor as a function of time for the run used in Fig. 9. Fluctuations are due to Poisson noise, as motion of the particles alters coefficients in the potential expansion.

virial quantity $-2T/W_c$ for the run used to produce Figure 9, where T is the total kinetic energy and W_c is the virial of Clausius defined by

$$W_c = \sum_k m_k \boldsymbol{x} \cdot \ddot{\boldsymbol{x}} . \tag{5.17}$$

(Recall that W_c is the appropriate quantity to use to compute the virial theorem for an arbitrary force law rather than the potential energy of the system [e.g., White 1982; Sellwood 1987].) In virial equilibrium $-2T/W_c \equiv 1$. Note from Figure 13 that for the SCF approach this condition is not satisfied. The quantity $-2T/W_c$ shows irregular time-variability over a range of time scales. The amplitude of these variations is $\lesssim 1\%$, in good agreement with what one might expect from $N^{1/2}$ fluctuations with $N = 10^4$ particles. (Note, however, that these variations do not lead to a secular change in $-2T/W_c$.) Although local two-body interactions are unimportant in SCF methods, oscillations induced by global fluctuations in particle density give rise to time-dependent effects that mimic a sort of two-body relaxation phenomenon. Since the violation of energy conservation of individual particle orbits is similar in SCF methods, spherical harmonic expansion techniques, and tree-codes, we conclude that these global effects dominate relaxation in three-dimensional particle systems with moderate N, when forces are softened. The ultimate cause of the fluctuations is Poisson noise. With a given number of particles, N, to define coefficients they will differ from their true values of $\sim O(N^{-1/2})$. Since these deviations are not strongly correlated in time, the implied fluctuations in the potential cause energy changes in a diffusive fashion.

At first sight, the results shown in Figures 6–13 and Tables 1 and 2 are slightly discouraging. However, one should recall that the SCF method is significantly more efficient than, say, a tree-code. For $N = 10^4$, with the parameters used to generate Figures 6 and 8, the tree-code is approximately 165 times slower than the SCF code on a Cray Y-MP. This ratio would increase to nearly 250 for runs involving 10^6 particles since the SCF technique is linear with particle number while tree-codes scale as $\sim O(N \log N)$. Of course, the calculation shown in Figure 6 was performed with a small number of basis functions. For typical applications we anticipate that the SCF method will be $\sim$10–100 times faster than a tree-code. Thus, for *fixed cpu costs*, even the most basic implementation of the SCF algorithm will suppress relaxation effects by at least a factor $\sim$3–10 relative to tree-codes, provided, of course, that the dynamical phenomenon being investigated can be adequately resolved with only a few basis functions. We say "at least" because the SCF method is, on average, somewhat better at suppressing relaxation noise than the other codes we have tested. For general values of $l_{\max}$, Tables 1 and 2 imply that particles' energy and angular momenta are conserved more accurately in the SCF approach than the others by $\sim$50–100%. For perfectly spherical models ($l_{\max} = 0$) our method is clearly better than the others listed in Tables 1 and 2.

5.4. *Temporal Smoothing*

The mean-field nature of the SCF method suggests a possible refinement that may mitigate relaxation effects significantly. Consider Figure 14, which shows the lowest order expansion coefficient in a run identical to that in Figure 13, but in which only the lowest order basis function has been retained ($n_{\max} = 0$ and $l_{\max} = 0$). The coefficient shown has been normalized so that it would be precisely unity in the continuum limit.

As can be seen from Figure 14, the expansion coefficients in the SCF technique undergo irregular fluctuations in time as the result of $N^{1/2}$ sampling errors. In addition, in this particular example A'_{000} is offset from its true value by $\sim$0.8%, mainly because the density field is poorly sampled at small radii. It is the irregular fluctuations in A'_{000} that give rise to nonconservation of individual particle energies. If A'_{000} were constant in time but not equal to one, particle energies would be strictly conserved but they would not be equal to their continuum limits.

Figure 14 motivates a modification to the SCF method that would be impossible or, at best, very difficult to implement in N-body codes, which we refer to as "temporal smoothing." That is, one could imagine setting A'_{000} equal to the global time-average of the values plotted in Figure 14, and then integrating particle orbits in this fixed potential. As implied earlier, particle energies would

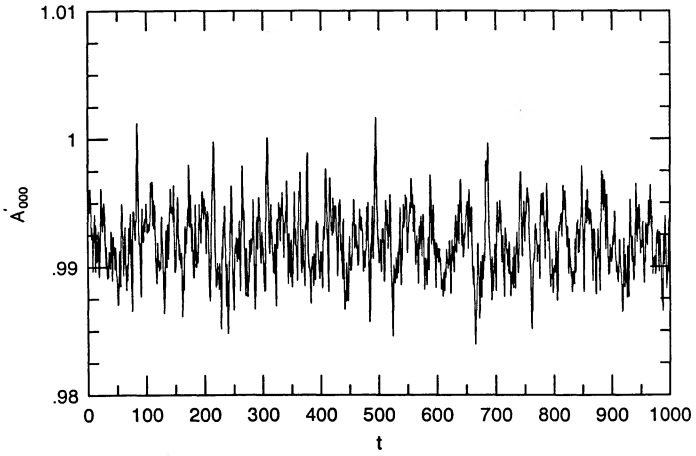

FIG. 14.—Expansion coefficient in a purely radial version of the run shown in Fig. 10, as a function of time. A'_{000} differs from the value of A_{000} given by eq. (2.33) by a constant factor so that A'_{000} would be precisely one in the continuum limit.

then be conserved to high accuracy and, aside from time-integration and round-off errors, there would be no relaxation. Naturally, such a drastic procedure is not justified if a signal is present in addition to the noise. A more suitable algorithm in that case would be to locally time-average the coefficients and then use these averaged quantities as inputs to a code which integrates orbits in a prescribed potential. If a sufficiently fine-tuned method for performing this temporal filtering could be found, it would be possible to effectively eliminate much of the discreteness noise responsible for relaxation but retain the physical response. Note that such a procedure is possible in the SCF method only because the fields are completely specified by the expansion coefficients which, although time-dependent, are not functions of the spatial coordinates. An analogous approach is not possible in N-body codes since they do not provide a mean-field description of the system.

5.5. *Stacking Models*

Another capability afforded by the SCF method is the possibility of stacking together different dynamical calculations in a way that cannot be done using direct N-body techniques. For example, one could perform a number of independent dynamical calculations with different initial conditions and tabulate the expansion coefficients in each as a function of time. Then, one could obtain a refined estimate of the time-dependence of the expansion coefficients by simply averaging together these tabulated functions at each output time. In principal, these averaged coefficients could be fed into the particle integrator and used to evolve the particles in a field which is effectively much smoother than that in any individual realization.

Since the fluctuations in the expansion coefficients, like those in Figure 14, result from Poisson noise, this stacking procedure will converge similarly to increasing the particle in a single simulation. That is, the noise level in a set of coefficients obtained by adding, say, 10 runs with $N = 1000$ would be the same as that in a single run with $N = 10{,}000$. Since the cpu cost of the SCF method is linear in N, stacking does not reduce the computer time needed to attain a given accuracy. It does, however, offer the possibility of effectively increasing N arbitrarily on machines with limited memory.

Another advantage of stacking is that it enables one to obtain an immediate quantitative estimate of the level of statistical noise by measuring moments of the distribution of coefficients computed from the different initial realizations, simultaneously with improving the accuracy of the integration. This cannot be done by appealing to a single run, irrespective of the number of particles used in that calculation.

6. DISCUSSION

The fundamental constituents of a collisionless system, such as stars in galaxies or electrons and ions in dense plasmas, move along orbits which are not perturbed by individual two-body interactions. A distinguishing characteristic of collisionless stellar objects is that the gravitational potential is essentially determined by their continuum mass distributions. Stars in a galaxy pass by one another with negligible effect and interact only indirectly in a mean-field sense. In other words, to a high degree of precision the gravitational field of a galaxy is independent of the relative coordinates of the mass entities which generate it. In cases where relaxation effects are non-negligible, as in small clusters of stars, the force on each object is determined by summing over all two-body interactions. Consequently, the potential depends explicitly on relative coordinates of stars.

The Vlasov equation cannot yet be solved by conventional finite-difference algorithms and a Monte Carlo approach is generally used to compute the evolution of collisionless systems. The bottleneck in codes based on this technique lies in calculating the potential of each particle in a self-consistent manner. In "N-body" algorithms, the potential is computed as if the actual system were composed of N discrete entities and, consequently, it depends explictly on the relative coordinates of these "particles." Softening is introduced into this method to prevent strong interactions between the particles, somewhat reducing the effects of two-body encounters.

In our opinion, the N-body approach does not obviously represent the optimal strategy to simulate collisionless dynamics; it appears more natural to use a formulation in which individual particles do not interact with one another directly. One such class of techniques comprises the self-consistent field (SCF) method, in which the fields are expanded in complete basis sets. The potential in SCF codes does not depend on relative coordinates of particles, provided that the expansions are truncated at low-order, and, hence, does not require the introduction of unphysical softening. For these reasons, SCF algorithms are closer in spirit to the dynamics of collisionless systems than are N-body methods. Computationally, after the potential is determined, one integrates N one-body orbits in a given gravitational field; a procedure well-suited for modern heavily parallelized computer architectures. With an improved density, as determined from these orbits, a new potential can be found which may allow one to converge self-consistently to the true collisionless limit.

To maximize efficiency, it is desirable to select a basis in which the lowest order terms provide a good approximation to the system being studied. By truncating the expansions at relatively low order, it is possible to obtain good global accuracy while not resolving small-scale irregularities. Some early implementations of the basis function method made use of spherical harmonics to expand the angular dependence, but solved the radial equation in closed form (e.g., van Albada & van Gorkom 1977; Villumsen 1982; White 1983; McGlynn 1984). As a consequence of this inconsistency, "spherical harmonic codes" retain essential characteristics of N-body techniques A mean-field description requires that the radial dependence also be expanded in basis functions.

In this paper we have presented a formulation of the SCF method in which the lowest order member of the basis sets resemble the structure of a galaxy obeying the $R^{1/4}$ law in projection. Our scheme is similar to that suggested by Clutton-Brock (1973) for systems well-represented by a Plummer model. As with all such algorithms, the primary disadvantage of our technique is its inflexibility. The basis set derived here will not be useful for modeling objects whose projected densities differ substantially from the de Vaucouleurs law. In addition, the particular approach used here and by Clutton-Brock does not lend itself easily to other density distributions. For example, it might be of interest to obtain similar formulations for either the modified Hubble profile (Binney & Tremaine 1987)

$$\rho(r) = \rho_0 \frac{1}{(1 + r^2)^{3/2}} \tag{6.1}$$

or for Jaffe's model (Jaffe 1983)

$$\rho(r) \propto \frac{1}{r^2(1+r)^2} . \tag{6.2}$$

The former gives a good fit to the light distribution in elliptical galaxies while the latter is well-suited for mass distributons with strongly divergent central densities. However, the potentials for both the modified Hubble profile and for Jaffe's model depend logarithmically on radius, and, so, it is not immediately obvious how to generalize the potential to higher order *lm* pairs, as in equation (2.11). The expansions given here and by Clutton-Brock succeed because both the lowest-order density and potential are simple algebraic functions of radius.

Our method may, however, be very appropriate for modeling the dynamics of systems that are nearly isothermal over some range in radius. This expectation follows from the fact that the rotation curve of the model studied by Hernquist (1990a) is approximately flat at intermediate radii $a \ll r \ll \infty$. The circular velocity associated with the density profile of equation (2.1) is

$$v_c = \frac{\sqrt{GMr}}{r+a} , \tag{6.3}$$

Hernquist (1990a). Note that $v_c \sim r^{1/2}$ as $r \to 0$ and $v_c \sim r^{-1/2}$ as $r \to \infty$. Simulations of the formation of galactic halos (Dubinski & Carlberg 1991) show that this rotation curve provides a good approximation to those of actual galaxies provided that the scale length a is sufficiently large. One approach, then, for modeling the dynamics of an elliptical galaxy surrounded by a dark matter halo would be to represent each component by the model in equation (2.1) but select different scale lengths for the luminous and dark matter. An example is shown in Figure 15, where we plot v_c computed for a composite system consisting of a galaxy and a dark matter halo:

$$v_c^2 = v_{c,\mathrm{gal}}^2 + v_{c,\mathrm{halo}}^2 = \frac{GM_{\mathrm{gal}}r}{(r+a_{\mathrm{gal}})^2} + \frac{GM_{\mathrm{halo}}r}{(r+a_{\mathrm{halo}})^2} , \tag{6.4}$$

where we take $M_{\mathrm{gal}} = 10^{11}\ M_\odot$, $a_{\mathrm{gal}} = 2$ kpc, $M_{\mathrm{halo}} = 2 \times 10^{12}\ M_\odot$, and $a_{\mathrm{halo}} = 30$ kpc. This choice of scale length for the galaxy corresponds to an effective radius of approximately 3.6 kpc (see § 2.1). As can be seen from Figure 15, the rotation curve of this model is very nearly flat over a significant radial interval. In fact, v_c varies by only about 5% between 3 kpc $\lesssim r \lesssim$ 50 kpc. For most practical purposes, it would be difficult to distinguish such a rotation curve from those of actual galaxies. From a computational point of view, the generalization of the method discussed here to more than one component is trivial since the field equations are linear. Thus, it would be quite straightforward to model a system with a rotation curve like that in Figure 15 using our basis set. Specifically, one could expand the potential of each component in its own basis set and represent the interaction between the two as external fields.

For flattened models with exponential density distributions a Fourier-Bessel expansion in cylindrical coordinates is appropriate. We refer the reader to the paper by Villumsen (1985) for an implementation of this technique in the context of numerical simulation.

In spite of its limitations, we anticipate that the SCF method presented here will have a wide range of scientific application. Of particular interest are situations where an accurate treatment of individual orbits is critical and others where the evolution occurs slowly over many dynamical times. Among these are the response of dwarf galaxies to tidal perturbations (e.g., Kuhn & Miller 1989; McGlynn 1990), the growth of central black holes and their effect on the large-scale properties of elliptical galaxies and bulges (e.g., Gerhard & Binney 1985; Norman et al. 1985; Hasan & Norman 1990), instabilities in models of elliptical galaxies (e.g., Merritt & Aguilar 1985; Barnes et al. 1986; Merritt & Hernquist 1991; Weinberg 1991), the orbital decay of satellites (e.g., White 1983; Lin & Tremaine 1983; Bontekoe 1988; Hernquist & Weinberg 1989), and coupling between bars and halos (e.g., Little & Carlberg 1991). Many of these problems involve subtle orbital dynamics that we suspect cannot be adequately addressed with conventional N-body

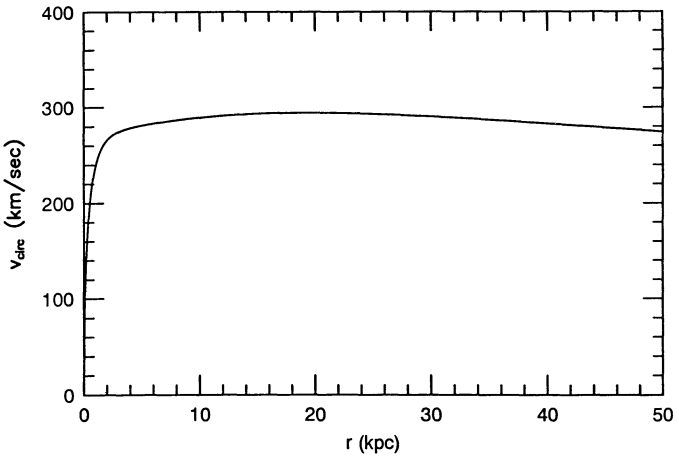

FIG. 15.—Representative rotation curve resulting from superposition of two models with the density profile of eq. (2.1). The smaller component (galaxy) has a mass $M_{\mathrm{gal}} = 10^{11}\ M_\odot$ and a scale-length $a_{\mathrm{gal}} = 2$ kpc. The larger component (halo) has a mass $M_{\mathrm{halo}} = 2 \times 10^{12}\ M_\odot$ and a scale length $a_{\mathrm{halo}} = 30$ kpc.

codes. Two-body effects scatter orbits from one family to another, masking redistribution of orbits by, e.g., a central point mass (Norman, May, & van Albada 1985). The long-term response of galaxies to tides, orbital decay of satellites, and bar-halo coupling depend upon resonant interactions between orbits and time variations in the potential (Tremaine 1981; Tremaine & Weinberg 1984; Weinberg 1986). Fluctuations in the phase-space distribution of particles owing to discreteness noise may artificially broaden resonances and contaminate the response. A rigorous treatment of collisionless stellar dynamics, therefore, demands that unphysical effects such as these be eliminated to the greatest extent possible. While it is not yet proven that SCF methods like those presented in this paper can suppress relaxation to such a degree, we believe that they offer one of the best computational approaches to collisionless stellar dynamics.

A particularly fruitful avenue of future research is the implementation of SCF methods on massively parallel computers like the Connection Machine (see, e.g., Hillis 1985; Hillis & Barnes 1987). Owing to the decomposition of the potential computation and force evaluation into N one-body problems, ideal load-balancing will be possible on parallel architectures. Factors ~ 10–30 improvement over Crays should be attainable with existing technology. The explosive growth of parallel computing suggests, therefore, that an additional factor ~ 100 may be possible within the next ~ 5 yr. In that event, dynamical simulations employing $N \sim 10^{10}$–10^{11}, which is similar to the number of stars in an actual galaxy, will be feasible in the near future.

We are particularly grateful to James Binney for his careful reading of the manuscript and many cogent comments on its contents. We also thank Josh Barnes, Martin Schwarzschild, Jerry Sellwood, and Martin Weinberg for enlightening discussion. This work was supported in part by an allocation of Cray time from the Pittsburgh Supercomputing Center, the Alfred P. Sloan Foundation, NASA Theory grant NAGW-2422, NSF grants AST 90-06958 and AST 90-18526, and California Space Institute grants CS 79-90 and CS 47–91.

REFERENCES

Aarseth, S. J. 1967, Bull. Astron., 3, 47
Abramowitz, M., & Stegun, I. A. 1972, Handbook of Mathematical Functions (New York: Dover)
Allen, A. J., Palmer, P. L., & Papaloizou, J. 1990, MNRAS, 242, 576
Aoki, S., & Iye, M. 1978, PASJ, 30, 519
Barnes, J. E., Goodman, J., & Hut, P. 1986, ApJ, 300, 112
Barnes, J. E., & Hut, P. 1986, Nature, 324, 446
Binney, J., & Tremaine, S. 1987, Galactic Dynamics (Princeton: Princeton Univ. Press)
Bontekoe, T. R. 1988, Ph.D. thesis, Groningen
Bontekoe, T. R., & van Albada, T. S. 1987, MNRAS, 224, 349
Clutton-Brock, M. 1972, Ap&SS, 16, 101
———. 1973, Ap&SS, 23, 55 (CB)
de Vaucouleurs, G. 1948, Ann. d'Astrophys., 11, 247
de Zeeuw, T. 1985a, MNRAS, 216, 273
———. 1985b, MNRAS, 216, 599
Dongarra, J. J. 1991, Univ. Tennessee technical report
Dubinski, J., & Carlberg, R. G. 1991, Univ. Toronto preprint
Fridman, A. M., & Polyachenko, V. L. 1984, Physics of Gravitating Systems, Vol. 2 (New York: Springer), 282
Fry, J. N., & Peebles, P. J. E. 1980, ApJ, 236, 343
Gerhard, O. E., & Binney, J. 1985, MNRAS, 216, 467
Hasan, H., & Norman, C. 1990, Space Telescope Science Institute preprint, No. 428
Hénon, M. 1964, Ann. d'Astrophys., 27, 83
Hernquist, L. 1987, ApJS, 64, 715
———. 1990a, ApJ, 356, 359
———. 1990b, J. Comput. Phys., 87, 137
Hernquist, L., & Barnes, J. E. 1990, ApJ, 349, 562
Hernquist, L., & Katz, N. 1989, ApJS, 70, 419
Hernquist, L., & Weinberg, M. D. 1989, MNRAS, 238, 407
Hillis, W. D. 1985, The Connection Machine (Cambridge: MIT Press)
Hillis, W. D., & Barnes, J. 1987, Nature, 326, 27
Jackson, J. D. 1975, Classical Electrodynamics (New York: Wiley)
Jaffe, W. 1983, MNRAS, 202, 995
Kalnajs, A. J. 1976, ApJ, 205, 745
King, I. R. 1966, AJ, 71, 64
Kuhn, J. R., & Miller, R. H. 1989, ApJ, 341, L41
Lin, D. N. C., & Tremaine, S. 1983, ApJ, 264, 364
Little, B., & Carlberg, R. G. 1991, Univ. Cambridge preprint
McGlynn, T. A. 1984, ApJ, 281, 13
———. 1990, ApJ, 348, 515
Merritt, D., & Aguilar, L. A. 1985, MNRAS, 217, 787
Merritt, D., & Hernquist, L. 1991, ApJ, 376, 439
Merritt, D., & Stiavelli, M. 1990, ApJ, 358, 399
Norman, C. A., May, A., & van Albada, T. S. 1985, ApJ, 296, 20
Ostriker, J. P., & Bodenheimer, P. 1968, ApJ, 151, 1089
Ostriker, J. P., & Mark, J. W.-K. 1968, ApJ, 151, 1075
Ostriker, J. P., & Peebles, P. J. E. 1973, ApJ, 186, 467
Plummer, H. C. 1911, MNRAS, 71, 460
Press, W. H., Flannery, B. P., Teukolsky, S. A., & Vetterling, W. T. 1986, Numerical Receipes: The Art of Scientific Computing (Cambridge: Cambridge Univ. Press)
Schwarzschild, M. 1979, ApJ, 232, 236
———. 1982, ApJ, 263, 599
Sellwood, J. A. 1987, ARA&A, 25, 151
Sommerfeld, A. 1964, Partial Differential Equations in Physics (New York: Academic Press)
Szegö, G. 1939, Orthogonal Polynomials (New York: American Mathematical Society)
Toomre, A. 1963, ApJ, 138, 385
Tremaine, S. 1981, in The Structure and Evolution of Normal Galaxies, ed. S. M. Fall & D. Lynden-Bell (Cambridge: Cambridge Univ. Press), 67
Tremaine, S., & Weinberg, M. D. 1984, MNRAS, 209, 729
van Albada, T. S., & van Gorkom, J. H. 1977, A&A, 54, 121
Villumsen, J. V. 1982, MNRAS, 199, 493
———. 1985, ApJ, 290, 75
Weinberg, M. D. 1986, ApJ, 300, 93
———. 1989, MNRAS, 239, 549
———. 1991, ApJ, in press
White, S. D. M. 1982, in Morphology and Dynamics of Galaxies, ed. L. Martinet & M. Mayor (Sauverny: Geneva Observatory), 289
———. 1983, ApJ, 274, 53
Yabushita, S. 1969, MNRAS, 143, 231
Young, P. J. 1976, AJ, 81, 807